AD-758 216

USE OF ACOUSTIC EMISSION IN NONDESTRUC-
TIVE TESTING

Julian R. Frederick

Michigan University

Prepared for:

Air Force Materials Laboratory
Advanced Research Projects Agency

October 1972

AFML-TR-72-114

USE OF ACOUSTIC EMISSION IN NONDESTRUCTIVE TESTING

J. R. FREDERICK

COLLEGE OF ENGINEERING
DEPARTMENT OF MECHANICAL ENGINEERING
THE UNIVERSITY OF MICHIGAN

OCTOBER 1972

Approved for public release; distribution unlimited.

NOTICE

When Government drawings, specifications, or other data are used for any purpose other than in connection with a definitely related Government procurement operation, the United States Government thereby incurs no responsibility nor any obligation whatsoever; and the fact that the government may have formulated, furnished, or in any way supplied the said drawings, specifications, or other data, is not to be regarded by implication or otherwise as in any manner licensing the holder or any other person or corporation, or conveying any rights or permission to manufacture, use, or sell any patented invention that may in any way be related thereto.

AFML-TR-72-114

USE OF ACOUSTIC EMISSION IN NONDESTRUCTIVE TESTING

J. R. FREDERICK

COLLEGE OF ENGINEERING
DEPARTMENT OF MECHANICAL ENGINEERING
THE UNIVERSITY OF MICHIGAN

DOCUMENT CONTROL DATA - R & D

(Security classification of title, body of abstract and indexing annotation must be entered when the overall report is classified)

1. ORIGINATING ACTIVITY *(Corporate author)*	2a. REPORT SECURITY CLASSIFICATION
The University of Michigan Ann Arbor, Michigan 48104	Unclassified
	2b. GROUP NA

3. REPORT TITLE

Use of Acoustic Emission in Nondestructive Testing

4. DESCRIPTIVE NOTES *(Type of report and inclusive dates)*

Final Technical Report, July 1, 1968 - August 31, 1971

5. AUTHOR(S) *(First name, middle initial, last name)*

Julian R. Frederick

6. REPORT DATE	7a. TOTAL NO. OF PAGES	7b. NO. OF REFS
December 1971	90	35

8a. CONTRACT OR GRANT NO.	9a. ORIGINATOR'S REPORT NUMBER(S)
F33615-68-C-1703	NA
b. PROJECT NO. ARPA Order No. 1244	
c. Program Code No. 8D10	9b. OTHER REPORT NO(S) *(Any other numbers that may be assigned this report)*
d.	AFML-TR-72-114

10. DISTRIBUTION STATEMENT

Approved for public release; distribution unlimited.

11. SUPPLEMENTARY NOTES	12. SPONSORING MILITARY ACTIVITY Advanced Research Projects Agency monitored by Air Force Materials Laboratory, LLN, Wright-Patterson Air Force Base, Ohio

13. ABSTRACT A model based on the activation of dislocation sources has been developed for predicting the effect of microstructure on acoustic emission. The model predicts a minimum dislocation source length and slip distance below which no emission will be detected. Experimental results obtained on various metals and alloys having different microstructures substantiate the model. The effect of grain size on the acoustic emission from 99.99% aluminum and 99.9% copper suggests that macroscopic yielding in these metals occurs with the help of dislocation pile-ups that have been held up by grain boundaries and that the emission results from the activation of dislocation sources near the grain boundaries. Experimental results obtained under conditions of very low background noise level show that some metals produce acoustic emission when the applied load is removed. The amount of emission that is observed correlates with the magnitude of the Bauschinger effect in the metal. In those metals that show an "unload" acoustic emission effect there is the possibility of using it to investigate the magnitude of the residual stress in a specimen. Creep and fatigue phenomena can also be studied by the use of acoustic emission. However, for high strength materials the very low signal level for any events other than those associated with the final propagation of a crack make it difficult to obtain significant data that are useful for the purpose of predicting fatigue or creep life.

DD FORM 1473 (1 NOV 65)

iq

90

14. KEY WORDS	LINK A		LINK B		LINK C	
	ROLE	WT	ROLE	WT	ROLE	WT
Acoustic Emission						
Unload Emission						
Grain Size						
Residual Stress						
Dislocation-Related Model						
Materials Strength						

1b

FOREWORD

This is the final report on a study of the use of acoustic emission in nondestructive testing. This research is supported by the Advanced Research Project Agency of the Department of Defense and is monitored by the Air Force Materials Laboratory under Contract No. F33615-68-C-1703, initiated under ARPA Order 1244, Program Code 8D10. Captain J. W. Bohlen (AFML/LLN) is project engineer. This report covers the period from July 1, 1968 to August 31, 1971.

The program was carried out in the Rheology and Fracture Laboratories of the Mechanical Engineering Department at The University of Michigan. The work was under the direction of Professor J. R. Frederick. Professor David K. Felbeck has also participated in the program. Significant contributions to the program have been made by A.B.L. Agarwall, N. G. Sankar, and R. C. Fill, doctoral students in Mechanical Engineering at The University of Michigan. Other graduate students who have participated in the program are Charles Thomas, M. Shah, J. D. Harris, Lawrence Crum, William Bracht, and Arthur Birchenough.

This Technical Report has been reviewed and is approved.

THOMAS D. COOPER
Chief, Processing and
Nondestructive Testing Branch
Metals and Ceramics Division
Air Force Materials Laboratory

iii

ABSTRACT

A model based on the activation of dislocation sources has been developed for predicting the effect of microstructure on acoustic emission. The model predicts a minimum dislocation source length and slip distance below which no emission will be detected. Experimental results obtained on various metals and alloys having different microstructures substantiate the model. The effect of grain size on the acoustic emission from 99.99% aluminum and 99.9% copper suggests that macroscopic yielding in these metals occurs with the help of dislocation pile-ups that have been held up by grain boundaries and that the emission results from the activation of dislocation sources near the grain boundaries. Experimental results obtained under conditions of very low background noise level show that some metals produce acoustic emission when the applied load is removed. The amount of emission that is observed correlates with the magnitude of the Bauschinger effect in the metal. In those metals that show an "unload" acoustic emission effect there is the possibility of using it to investigate the magnitude of the residual stress in a specimen. Creep and fatigue phenomena can also be studied by the use of acoustic emission. However, for high strength materials the very low signal level for any events other than those associated with the final propagation of a crack make it difficult to obtain significant data that are useful for the purpose of predicting fatigue or creep life.

TABLE OF CONTENTS

TABLE OF CONTENTS (Concluded)

LIST OF ILLUSTRATIONS

LIST OF TABLES

I. INTRODUCTION

If there is an abrupt relaxation of either localized or long-range stresses within a solid material, strain waves are produced in the material that can be detected by means of a sensitive piezoelectric transducer attached to it. The noise that is produced is referred to as "acoustic emission." Most solid materials produce acoustic emission when they are loaded in tension and the following mechanisms have been suggested as sources of emission: the slip of dislocations, twinning, crack nucleation, and crack propagation.

This investigation is concerned with acoustic emission that originates from dislocation motion. This type of acoustic emission is usually one to two orders of magnitude less intense than the acoustic emission that results from crack propagation. An understanding of the acoustic emission resulting from dislocation motion is important because most plastic deformation of metals involves dislocation motion. Furthermore, all metals that fracture in a ductile manner will simultaneously deform plastically by means of the slip of dislocations. Hence a dynamic technique for studying dislocation motion offers the possibility of being a useful tool for investigating or monitoring deformation and fracture in metals.

If acoustic emission is to be used to monitor deformation and fracture processes it is important to know the effect of microstructure parameters on the acoustic emission process since the amount of dislocation related emission produced at any given stress level depends on the microstructure of the material. Parameters such as grain size, dislocation density, and the size and distribution of second-phase particles have been found to be important.

Theoretical models have been developed for explaining acoustic emission on the basis of dislocation motion and experiments have been performed to verify the models.

The acoustic emission also depends on whether or not a specimen had been previously loaded. Generally, a specimen will not give off acoustic emission until it has been stressed to a level that exceeds the previously applied stress. This characteristic is known as the "Kaiser" effect.

In some circumstances it is possible to observe acoustic emission when an applied stress is removed from a test specimen. This phenomenon has been observed in magnesium, a Cu-7.9% Al alloy, 70-30 brass, and several other materials. The effect appears to correlate with the magnitude of the Bauschinger effect in these materials.

The magnitude of the acoustic emission obtained on removing an applied stress depends on the magnitude of the applied stress, as well as on the type of material and its microstructure. Hence a measurement of the unload emission

1

offers a possible method of determining the residual stress level in a specimen that shows this effect. A model has been developed for this technique but the application to a practical situation is probably limited to one in which a simple stress state is involved.

Acoustic emission occurs during fatigue and creep in metals. Prior to crack nucleation the emission is of low level and due, at least in part, to dislocation motion. Various investigators have reported the results of tests in which acoustic emission has been monitored during fatigue or creep.[1-5]

Fatigue tests were planned for 7075-T6 aluminum, 6Al-4V titanium, and D6aC steel. Excessively high extraneous noise levels in the Research Incorporated 30,000 lb programmable fatigue machine on which it was planned to run the fatigue tests prevented completion of this phase of the effort.

A creep test was carried out on a 99.99% aluminum specimen at room temperature in which acoustic emission was observed during each of the three stages of creep. Two creep furnaces were set up for testing the 7075-T6 aluminum, 6Al-4V titanium and D6aC steel at temperatures and time intervals for which significant creep occurs in these alloys. Technical difficulties with external noise of unknown origin which occurred over extended periods of time made it impossible to obtain satisfactory data.

If acoustic emission is to be used as a nondestructive testing technique it usually requires that a stress be applied in some way. Furthermore, it is frequently desirable that this stress be applied so as to create as little extraneous noise as possible. Several methods for doing this were explored during the program. These are discussed in Section III.

II. THEORETICAL CALCULATIONS

A. A MODEL FOR DISLOCATION-RELATED ACOUSTIC EMISSION

In order to explain the sensitivity of dislocation-related acoustic emission to microstructure a model proposed by Agarwal[6] has been developed further and verified experimentally. This model is based on the activation of dislocation sources and the subsequent shutting off of the sources by the back-stress of piled-up dislocations.[7] The model is based on the assumption that below certain limits of free dislocation line length and dislocation glide distance there will be no detectable emission. These limits are determined by the strain sensitivity of the detection system, i.e., the minimum displacement δ_{min} at the surface of a test piece that can be detected by a piezoelectric transducer. This can be calculated from the following equation,

$$\delta_{min} = \frac{V_{min}}{g_{33}E_x} \tag{1}$$

where V_{min} is the voltage corresponding to the background noise level of the system, g_{33} is the piezoelectric stress constant of the transducer material, and E_x is the elastic modulus of the transducer material.

For the equipment used in this study V_{min} = 10 microvolts, g_{33} = 24.4 x 10^{-3} volt meter/newton, and E_x = 5.85 x 10^{10} newton/meter^2; hence, the minimum detectable displacement is

$$\delta_{min} = \frac{10 \text{ microvolts}}{24.4 \times 10^{-3} \times 5.85 \times 10^{10}} = 7.0 \times 10^{-15} \text{m}$$

In an aluminum specimen of 0.076 m (3.0 in.) deformed length, the average strain ϵ corresponding to this detectable displacement is

$$\epsilon = \frac{\delta_{min}}{\text{length}} = \frac{7.0 \times 10^{-15} \text{m}}{0.076 \text{ m}} = 9.1 \times 10^{-14}$$

If the probable losses in the system are considered, the minimum detectable levels of strain are probably one or two orders of magnitude larger.

The shear stress σ required to activate a dislocation source of initial length f is given by[8]

$$\sigma \simeq \frac{\mu b}{f} \tag{2}$$

where μ is the shear modulus of elasticity and b is the Burgers vector. Equation (2) represents here an average value for a combined edge and screw dislocation and is considered as being representative of those dislocations that can act as sources.

The number n of dislocations in the double pile-up that would be expected from a source that has been shut off by the back-stress of the piled-up dislocations has been shown to be[9]

$$n = \frac{(1-\nu)L\sigma}{\mu b} \simeq \frac{(1-\nu)L}{f} \tag{3}$$

where ν is Poisson's ratio and L is the total width of the pile-up. If the average glide distance of the dislocations in the pile-up is $3/4(L/2)$, the total area A_s swept out by n dislocations will be more than $n\pi(3L/8)^2$ but less than $n\pi(L/2)^2$; the latter value will be used in the calculations that follow. Thus if

$$A_s = n\pi\left(\frac{L}{2}\right)^2$$

then by the use of Eqs. (2) and (3),

$$A_s = \frac{\pi(1-\nu)L^3}{4f} \tag{4}$$

Assume that a tensile stress is applied axially to a simple cylindrical specimen of cross-sectional area A. For any given externally applied stress, those crystals that will first be subjected to slip will have nearly identical orientation to provide the maximum resolved shear stress for slip. Thus, those crystals that are subject to early slip can be treated in the same manner as a single crystal of total slip area A_s. Consider a slip system whose normal to the slip plane makes an angle φ with the applied tensile stress and whose slip direction lies at an angle λ to the applied tensile stress. The shear displacement δ_s at the end of the specimen that results from slip over an area A_s is

$$\delta_s = \frac{bA_s}{(A/\cos\varphi)}$$

The axial displacement δ_a is therefore

$$\delta_a = \delta_s \cos\lambda$$

If $\nu = 1/3$, and the value of $\cos\varphi\cos\lambda$ in the case of (111) [110] slip in aluminum is assumed to be $1/3$, then by the use of Eq. (4) the axial displacement at the end of an aluminum cylinder that results from the activation of a dislocation source is

4

$$\delta_a = \frac{\pi}{18} \frac{bL^3}{Af} \tag{5}$$

where b is Burgers vector for aluminum, L is the slip area diameter, f is the
dislocation source length, and A is the cross-sectional area of the specimen.
If Eq. (5) is combined with Eq. (1) for the minimum detectable strain, the fol-
lowing relationship between the slip region diameter L and source length f, both
in meters, is obtained:

$$L^3 = (4.5 \times 10^{-9} \text{ m}^2) \, f \tag{6}$$

The constant in Eq. (6) is based on a specimen area A of 31.7×10^{-6} sq m (0.049
in.^{2}) and a value of 2.86×10^{-10} m (2.86 Å) for the Burgers vector of aluminum.

Figure 1 shows a plot of Eq. (6) on a log-log coordinate graph. It defines
the minimum slip region diameter L that, with the equipment used and no attenu-
ation, will give detectable emission for a source of length f in an aluminum
specimen whose area is 31.7×10^{-6} sq m. Any values of L and f below the solid
line will not be detected in the system that has been postulated.

There are certain limitations on the ratio L/f. This places further limits
on the possible values of L and f. The length of a dislocation line that is
free to move is limited because of pinning either at the nodes of the disloca-
tion network or because of local defects such as hard particles. The maximum
possible glide distance for dislocations that are expanding out from a source is
also limited. If fine particles limit the glide distance to the order of 10f,
then L/f = 20. If the Frank network limits the glide distance, then L/f will
probably be closer to unity. A reasonable maximum value of L/f would be 20 for
the strains considered here. These strains are well below those corresponding
to the engineering yield stress. The solid line in Figure 1 provides a lower
boundary for detectable emission and the line L = 20f provides an upper boundary
for plausible slip systems that may operate in the microstrain region at stress
levels less than macroscopic yielding. The area bounded by these lines in Figure
1 is therefore the region where slip can be detected by acoustic emission with
the specimen size and transducer sensitivity that have been assumed in develop-
ing the model. The graph indicates that no acoustic emission should be detected
from sources having lengths of less than about 5×10^{-7} m (0.5μ).

B. EFFECT OF GRAIN SIZE ON DISLOCATION MOTION DURING MICROSTRAIN AND MACROSTRAIN

The plastic strain that metals undergo can be described as either micro-
strain or macrostrain. Strains of about 5×10^{-4} mark the general point at which
the transition from microplastic to macrostrain behavior occurs.

There is considerable uncertainty as to what mechanisms operate during the
microstrain regime and how important grain boundaries are as dislocation obstacles

5
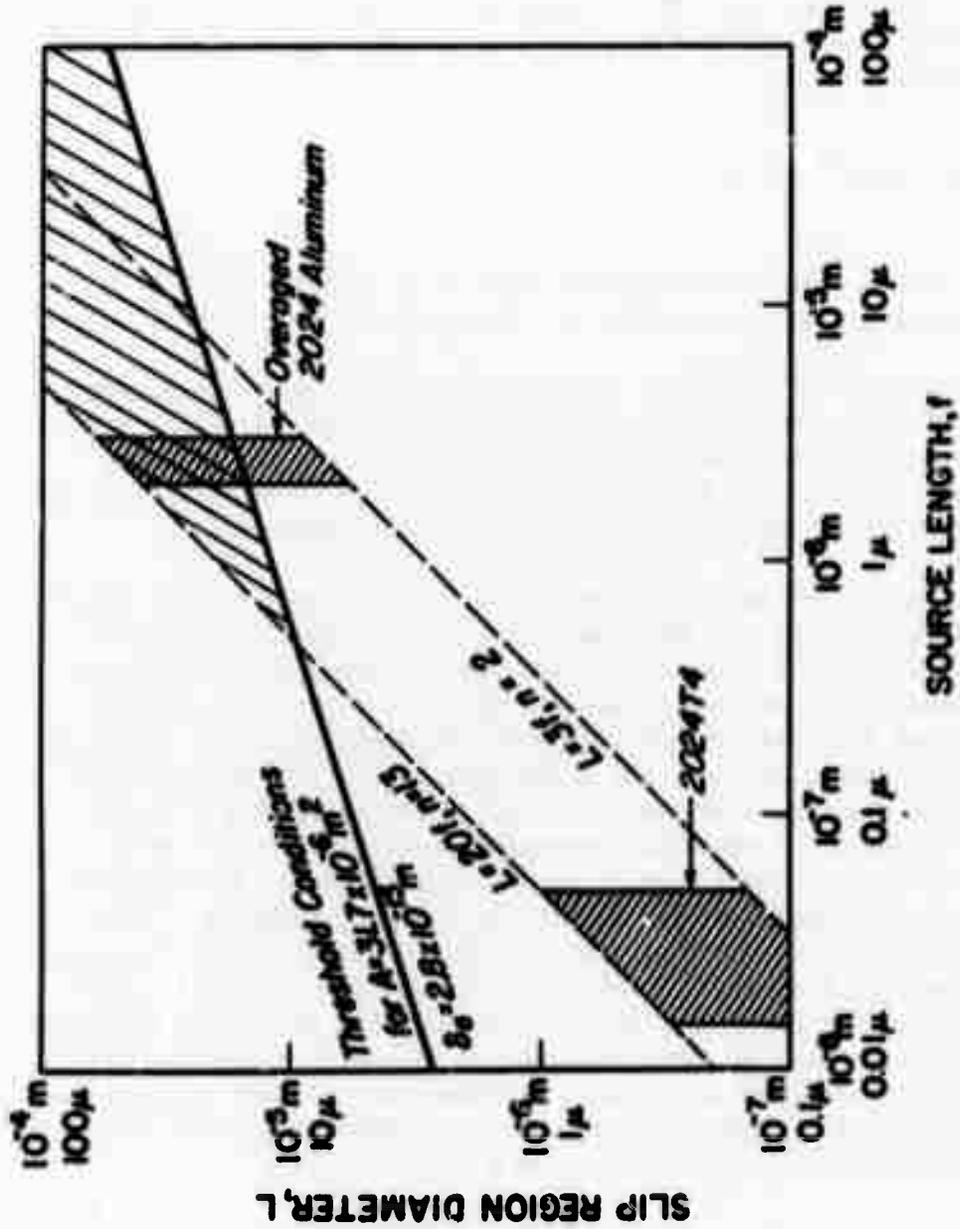
Figure 1. Relationship between slip region diameter L and source length ℓ for detectable acoustic emission. The region in which slip can be detected is shown by the coarse shading. For the model that is described it should be possible to detect acoustic emission for overaged 2024 aluminum alloy but not from the 2024-T4 alloy.

during microstrain. It is not known whether microstrain proceeds as the result of the movement of mobile or loosely pinned dislocation segments,[10] or by the activation of dislocation sources, or possibly both. The acoustic emission technique offers the possibility of providing some information concerning the processes involved during microstrain and the transition from microstrain to macrostrain.

In particular it is observed that the acoustic emission produced during microstrain is at a low-level and in the present study involving 99.99% aluminum it is independent of grain size. This supports the theory that the pinning and unpinning of dislocations is a possible source of acoustic emission.

The onset of macrostrain coincides with yielding and the amount of acoustic emission increases abruptly. On the basis of observed dislocation densities in 99.99% aluminum, it would be possible to obtain only 0.1% to 0.2% strain without the occurrence of dislocation multiplication. However, the observed rate of acoustic emission in 99.99% aluminum is roughly proportional to strain up to strains of 2%, and the proportionality factor is strongly dependent on grain size. Hence, dislocation multiplication provides a good explanation as to the source of the acoustic emission.

A model for microstrain has been suggested by Bilello and Metzger.[11] They envision that microstraining proceeds in the following manner. Potentially mobile dislocation segments have a uniformly distributed activation stress σ_A, ranging from σ_0 at the onset of microstrain, to σ_I at the end of the microstrain range. The glide distance l_m of an activated segment is proportional to $(\sigma_A - \sigma_0)$. It is assumed that there are N_I potentially mobile dislocation segments per unit volume. Each stress increment $d\sigma_A$ activates a fraction, $(\sigma_A - \sigma_0 / \sigma_I - \sigma_0)$, of the N_I sources, and the glide distance is given by

$$l_m = \frac{l_I(\sigma_A - \sigma_0)}{(\sigma_I - \sigma_0)} \tag{7}$$

where l_I is the maximum glide distance at the end of the microstrain range. These assumptions lead to a relationship in which the microstrain is proportional to the applied stress.

Experimental data obtained by Bilello and Metzger[11] on 99.99% Cu verify this relationship in the microstrain range and show that the strain is independent of grain size.

Microstrain therefore ends when a substantial fraction of the primary segments undergo forward motion, and an overlapping of clear zones of adjacent segments occurs. Thus, the end of the microstrain range occurs at a strain that is dependent on initial dislocation density.

The theoretical strength of a grain boundary depends on the mechanism by which dislocations are envisioned to cross the boundary. These mechanisms are

7

discussed by Li[12] who shows how they explain the rather universally valid
Petch Equation,

$$\sigma = \sigma_o + K\ell^{-1/2} \qquad (8)$$

where K is the "Petch slope," ℓ is the grain size, and σ is the yield stress.
The value of K is given by Hall and Petch as

$$K = \left[\frac{\sigma_1 \mu b \ell}{\pi(1-\nu)\ell_p}\right]^{1/2} \qquad (9)$$

where σ_1 is the strength of a grain boundary, ℓ_p is the pile-up length, b is
Burgers vector, μ is the shear modulus, and ν is Poisson's ratio. If the as-
sumption is made that $\ell_p = \ell/2$ or some other fraction of ℓ, then K is not a
function of grain size.

A mechanism proposed by Cottrell[36] suggests that slip in one grain ini-
tiates slip in a neighboring grain. Suppose that a dislocation pile-up is held
up by a grain boundary. One can then envision a Frank-Read source located a
distance ℓ_s from the boundary in the nieghboring grain exerting stress σ_p across
the boundary. The following relation for K is obtained:

$$K = \sigma_p(\ell_s)^{1/2}, \qquad (10)$$

This is in conformity with one interpretation[7] of the Petch equation which
postulates that yielding occurs in a polycrystal when the stress at the head of
a pile-up becomes large enough to activate a hypothetical Frank-Read source in
the neighboring grain, a distance ℓ_s from the grain boundary.

The effects of grain boundaries and other microstructure parameters on
acoustic emission have been studied experimentally in this investigation. The
results of this effort show that at the onset of macrostrain (yielding) there
is an abrupt increase in acoustic emission as well as strain. The effect on
acoustic emission is strongly grain size dependent in 99.99% aluminum. This is
consistent with a dislocation source activation model in which the dislocation
glide distance is limited to the size of the grains. In age hardened materials
the glide distance is limited by the size and spacing of the precipitated par-
ticles.

C. A MODEL FOR THE DETERMINATION OF RESIDUAL STRESS BY ACOUSTIC EMISSION

Acoustic emission measurement offers a possible method for the determina-
tion of the magnitude of the residual stress in materials that show negligible

8

load emission but a significant amount of unload emission. The basis for the method is as follows.

The amount of emission from a test specimen is related to the stress level, and to the volume of material stressed. For many engineering materials, including steel and aluminum, the emission is found to have the following characteristics:

(1) On repeated loading of a test specimen to a stress below its yield stress the rate of emission is essentially constant and low. The total emission produced on loading to a particular stress level is proportional to the applied stress, as shown in curve "o-a" in Figure 2.

(2) During the unloading part of the cycle the acoustic emission increases in an exponential manner as shown by the part of the curve "a-b" in Figure 2. The manner in which this unload emission might be used to determine the magnitude of residual stress is as follows.

Consider an idealized situation in which there is a region of uniform tensile stress and a region of uniform compressive stress, both of the same magnitude, as shown in Figure 3. Figure 4 shows the stress levels reached as a result of applying a tensile load "F" to this specimen. Figure 5 shows the separate cumulative emission from sections A and B of the model in Figure 3. Figure 6 is a combined cumulative emission curve.

If a large enough stress is applied to the specimen so that the section that was originally in compression is now subjected to a tensile stress, the cumulative emission curve would appear as shown schematically in Figure 7.

Hence, in a general case it is necessary to apply a tensile or compressive stress larger than the residual stress and then to observe the shape of the load and the unload cumulative acoustic emission curves. If a curve such as is shown in Figure 7 is obtained, the change in the slope of the load and unload curves will occur at the peak value of the residual stress.
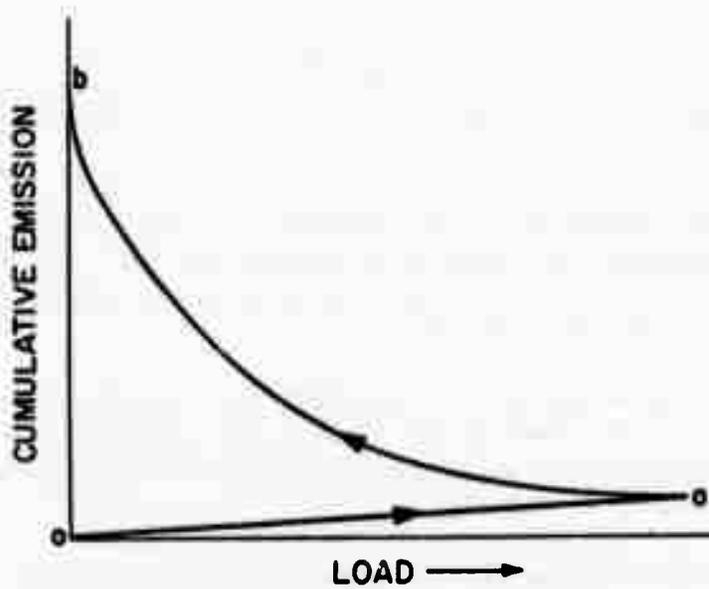
Figure 2. Repeated loading of a test specimen to stress levels below the yield stress results in the type of cumulative emission vs. load curve shown in the figure.

Figure 3. Simplified model for a specimen containing uniform compressive and tensile stresses. Region A is in tension. Region B is in compression.
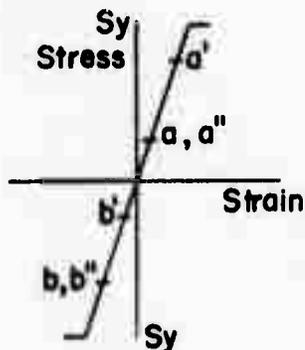
Figure 4. Stress levels applied to the specimen shown in Figure 3 in order to obtain the acoustic emission response shown in Figure 5.

10
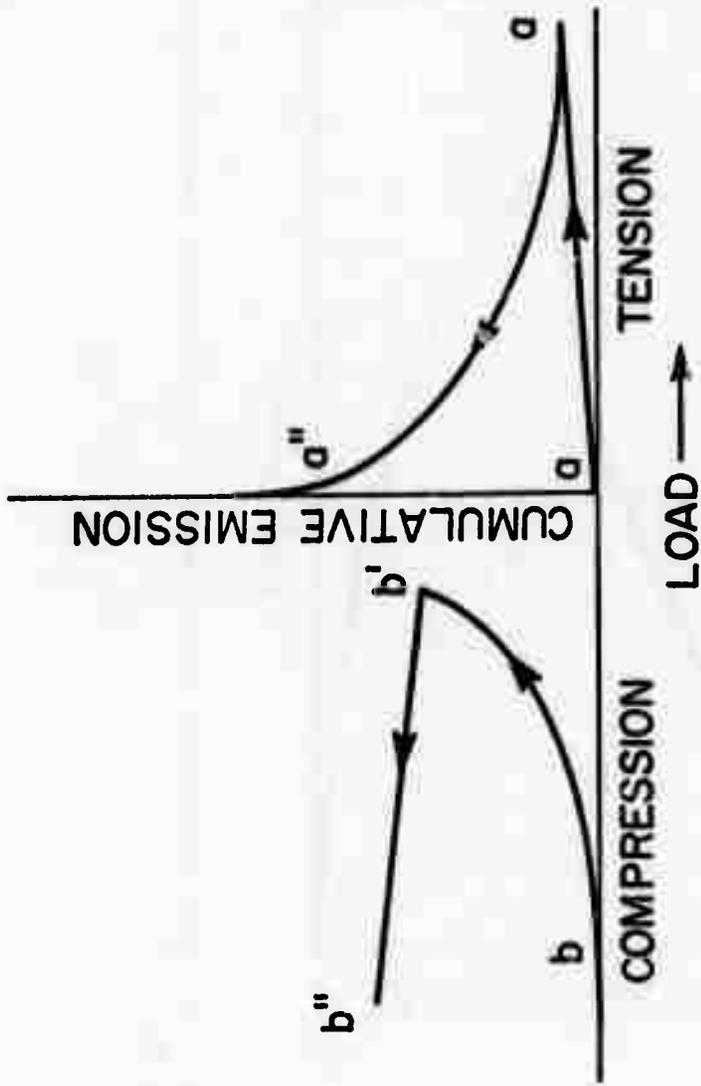
Figure 5. Schematic diagram of the acoustic emission from the model shown in Figure 3. Region A emits in the manner shown for the tensile loading. Region B emits in the manner shown for the compressive loading.

11
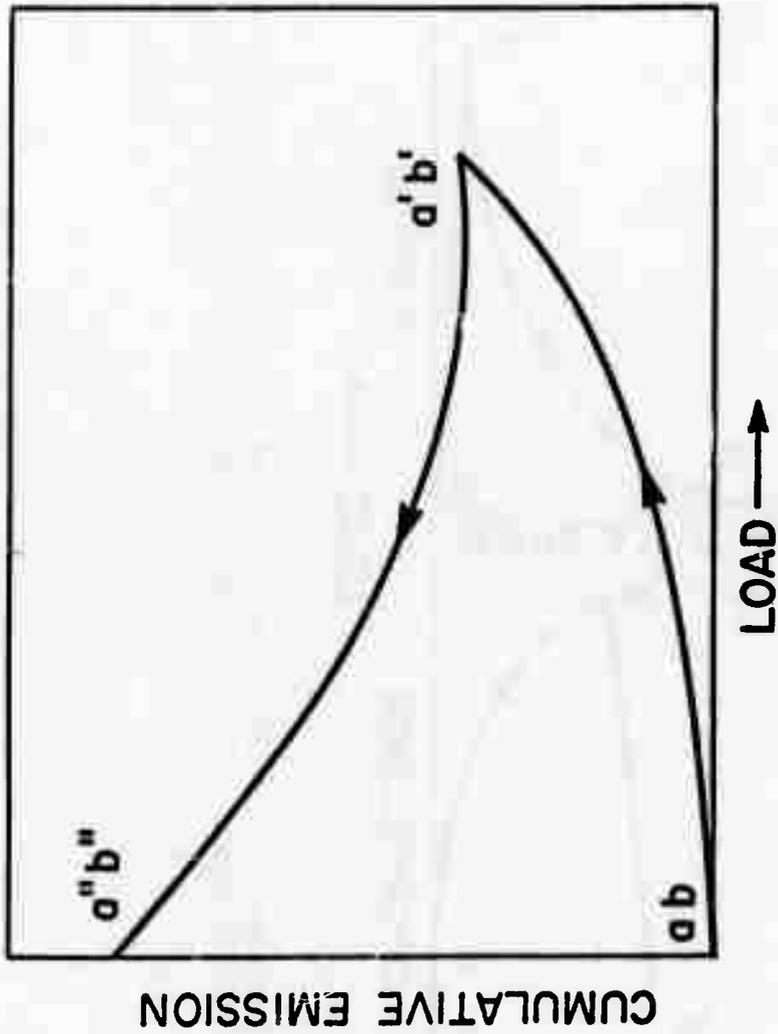
Figure 6. The combined emission for the model in Figure 3 is a combination of the two curves shown in Figure 5.
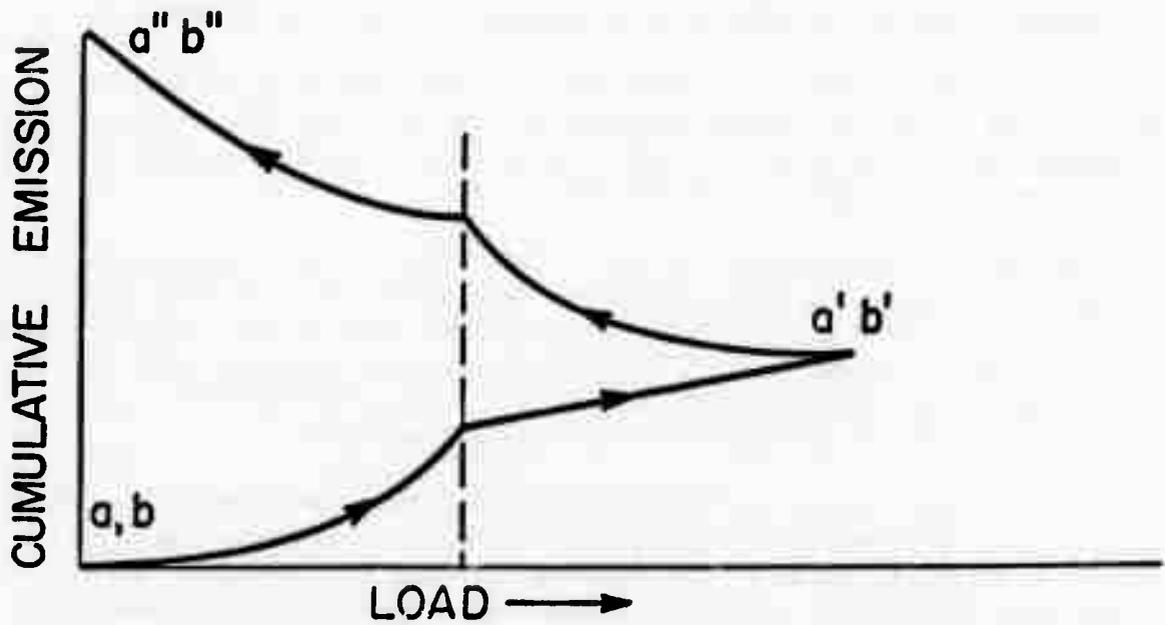
Figure 7. If a sufficiently large tensile stress is applied to the specimen shown in Figure 5 so that the region under compression is put into tension, a cumulative emission curve having two points of inflection should result.

III. EXPERIMENTAL PROCEDURES

A. INVESTIGATION OF THE EFFECTS OF MICROSTRUCTURE ON ACOUSTIC EMISSION

A detailed description of the electronic equipment is given in Ref. 19. Except where noted, all testing was done in the 100 to 300 kHz frequency range. A Dunegan DRC 02 transducer was used to detect the acoustic emission. Figure 8 shows a schematic diagram of the equipment.

The overall background noise had an rms value of about 6 microvolts at the preamplifier input. The amplitude of the smallest pulse to be registered on the counter was controlled by setting the trigger level of the counter. Normally, a trigger level setting of 0.1 V was used for testing purposes, which meant that a signal had to have an amplitude of 0.1 V or greater at the counter, or ten microvolts at the preamplifier input to be registered.

The load was applied to the specimen by the float and lever system shown in Figure 9. This was located inside an audiometric room which had a noise reduction capability of 60 dB for an octave band of 4800-9600 Hz. The low noise level preamplifier was also located inside the audiometric chamber and adjacent to the test specimen so that the input lead to it is short.

The materials tested were 99.99% aluminum supplied by the Aluminum Company of America, 2024 and 6061 aluminum alloys, copper-7.9% aluminum alloy, 70-30 brass, 99.95% magnesium, and 99.9% copper. All these materials are of fcc structure except the magnesium which is hcp. All the samples were polycrystalline. The compositions of the various materials tested are shown in Table 1.

Round specimens having a gauge section about 3 in. long and 1/4 in. in diameter were used in all tests except the grain size studies. Flat specimens with a 1 in. gauge length and a 1/4 x 1/8 in. cross-section were used in the grain size investigation.

B. RESIDUAL STRESS TESTS

Residual stress tests were performed on 1018 steel specimens and on 6061-T6 aluminum. The steel specimens were annealed at 950°F for three hours and the aluminum was tested in the T-6 condition.

The 6061-T6 aluminum specimens were 0.5 in. in diameter 4.0 in. long and had flat surfaces 1.5 in. long and 0.1 in. deep milled on both sides. One of these was tested in the "as-received" condition. Residual stresses were introduced in the other specimen by bending it to an angle of about 1/2 degree and then straightening it.

14
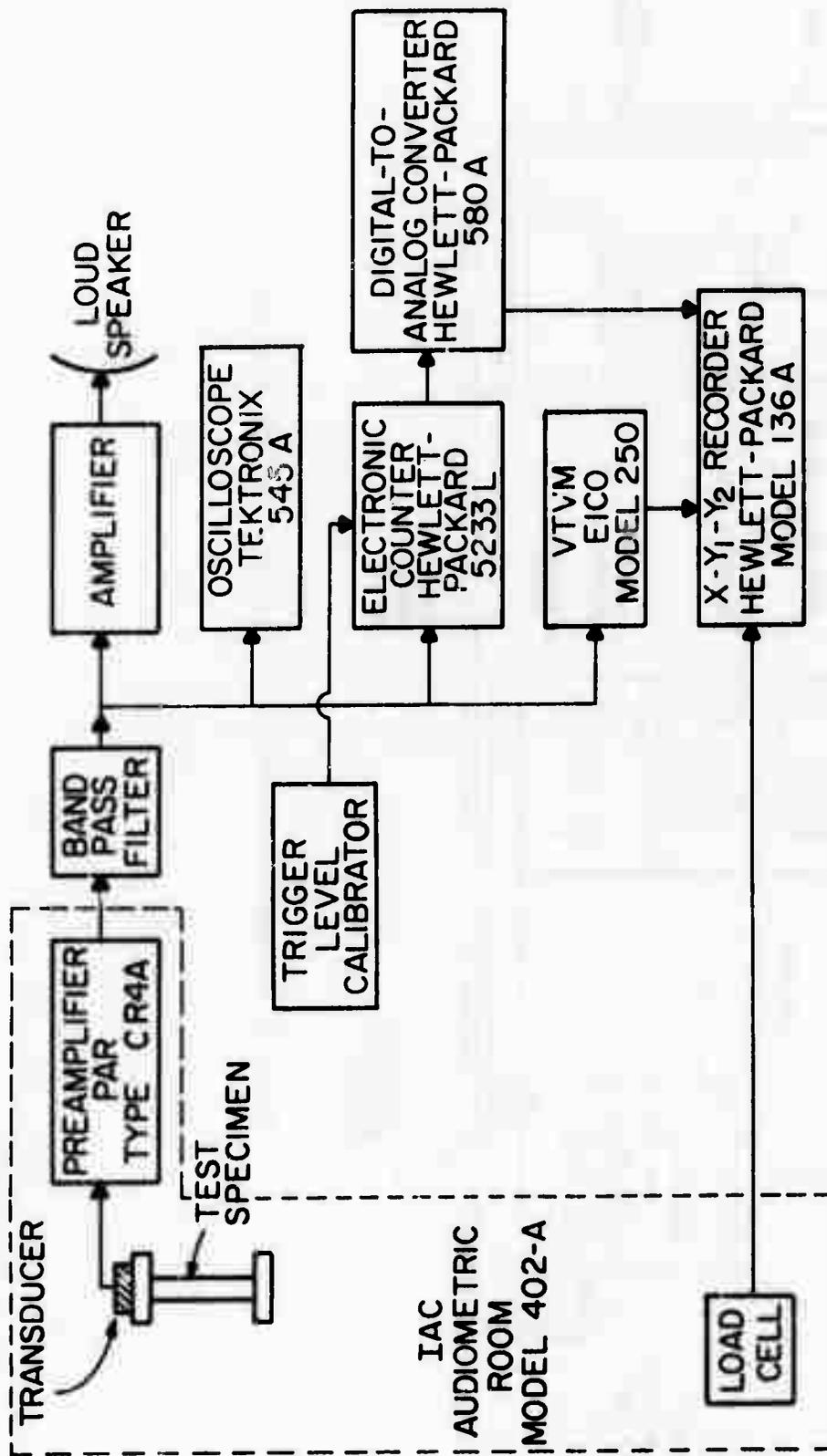
Figure 8. Block diagram of the electronic components used in the investigation.

15

* indicates that acoustic isolation or mismatch material is used.
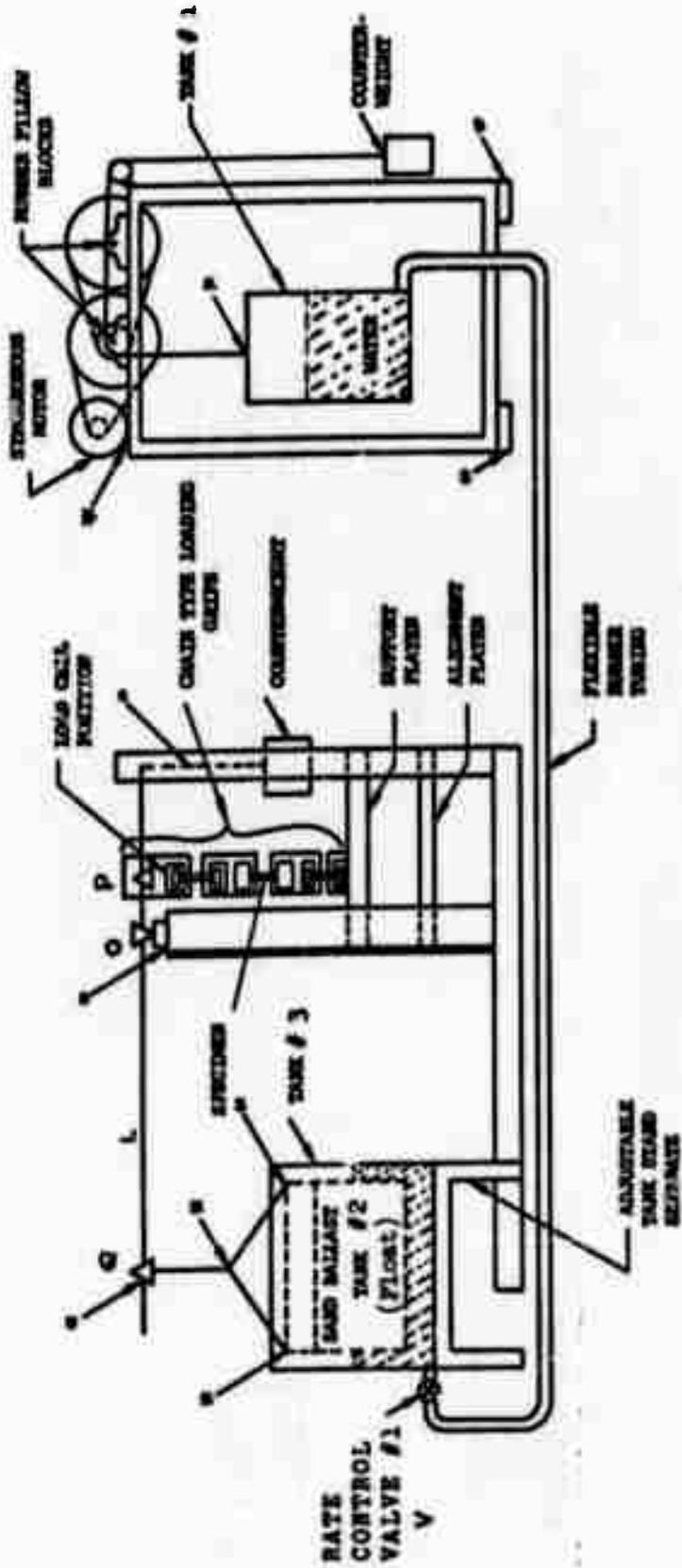
Figure 9. Schematic of the acoustic tensile testing machine.

16

TABLE I

COMPOSITIONS OF THE MATERIALS USED

(a) Aluminum and aluminum alloys

Type	Cu	Fe	Si	V	Zn	Mn	Mg	Cr	Al
99.99%	0.003	0.004	0.001	0.001	0.001	---	---	---	bal
6061 alloy	0.25	---	0.6	---	---	---	1.0	0.25	bal
2024 alloy	4.5	---	---	---	---	0.6	1.5	---	bal

(b) Magnesium*

Type	Al	Fe	Mn	Ni	Si	Ca	Zn	Mg
99.95%	0.03	0.036	0.03	0.001	0.01	0.01	0.02	bal

*The percentage impurities indicated in the table were the maximum allowable values.   99.95% was the minimum gauranteed purity.

(c) Copper-aluminum alloy

Aluminum*	7.6%
Copper*	bal.

*Prepared from stock of 99.99+% purity.

(d) 70-30 brass

Lead	0.07
Iron	0.05
Other elements	0.15
Copper	68.5
Zinc	bal

Three flat specimens of annealed 1018 steel were prepared having a gage section 5/8 in. wide, 1/4 in. thick and 4 in. long. Rectangular slots 1 in. long and 1/4 in. wide were cut in the center of two of the specimens. A 1018 steel insert 0.0015 in. longer than the slot was shrunk fit into the slot of one specimen. The slot in the other specimen was filled with an insert that was 0.002 in. thicker than the specimen. The specimen was then rolled until the insert was the same thickness as the specimen. The compressive stress produced in the insert in this way was reduced subsequently by plastically straining the main body of the specimen in a standard tensile machine. The stresses in the inserts were then measured by the use of strain gages placed on the inserts and applying sufficient tensile load so that no further change in the length of the insert occurred. These tests indicated that the compressive stresses were approximately 16,000 psi in the shrunk-fit specimen and 6,000 psi in the rolled-in specimen.

C. FATIGUE TESTS

Fatigue tests on 7075-T6 aluminum, D6aC steel, and 6Al-4V titanium were planned for a 30,000 lb load capacity, Research Incorporated, programmable testing machine using axial loading. This machine is hydraulically operated and utilized a feedback loop to control the applied load level. High background noise levels on this machine made it impossible to conduct any fatigue tests, however. A major source of noise appeared to be cavitation noise in the fluid that activated the ram in the machine. Various methods for obtaining acoustic isolation between the ram and the test specimen were attempted but not enough reduction of the noise was obtained to obtain reliable acoustic emission data in a fatigue test.

D. CREEP TESTS

A creep test was performed at room temperature on a 99.99% aluminum specimen in the sound isolated room used for studying the effect of microstructure on acoustic emission. The experimental setup is shown in Figure 9. The gauge section of the specimen measured 1/8 in. x 1/8 in. and had a length of 3 in. No difficulty was encountered in detecting acoustic emission during short time creep (less than one hour) in this specimen. Longer creep times were not attempted because the primary interest was in the elevated temperature tests of the higher strength alloys.

Two conventional elevated temperature creep units were set up and instrumented for acoustic emission tests on D6aC steel, 6Al-4V titanium, and 7075-T6 aluminum. Provision was made for locating the acoustic emission transducer outside of the furnace containing the test specimen and coupling it to the specimen by means of a metal rod or bar joined to the specimen.

18

E. THERMAL STRESSING

Several methods for inducing thermal stresses as a means of producing acoustic emission were tried. These were as follows: (1) an infrared heat lamp; (2) an 80 W laser beam; (3) heating a specimen and quenching it in an oil bath (taking care to avoid bubble formation); and (4) cooling by the use of a localized heat sink consisting of a small container filled either with liquid nitrogen or a "dry ice" and acetone mixture. In these tests the acoustic emission transducer was placed at a point on the specimen that was at room temperature or, in the case of the oil bath test, it was placed on the outside of the wall of the tank.

IV. EXPERIMENTAL RESULTS

A. ACOUSTIC EMISSION BEHAVIOR OF 99.99% ALUMINUM

Figure 10 shows the type of acoustic emission data obtained on annealed 99.99% aluminum. The X-Y recorder pen is automatically reset to zero after every 10,000 counts. This accounts for the appearance of the load emission plot for a total count of 20,800 during the first loading. The dashed arrow ($\updownarrow$) on the abscissa indicates the maximum stress level reached in the previous load-unload cycle. The other solid arrow ($\uparrow$) indicates the maximum stress level reached. There is a large amount of load emission of the high-rate type. The unload emission counts are very low and are of the burst type. Figure 11 shows stress-strain data for this material along with load and unload emission data.

Only very few load emission counts were obtained on the second loading when the previous stress level is not exceeded: 84 counts as compared to 20,800 counts in the first load cycle. The load emission activity of high-rate type commences on loading when the previous stress level is exceeded in the second loading. A preload of 37.5 lb was maintained on the specimen to minimize emission from the interface between the specimen and the grips.

Specimens with different grain sizes were obtained by cold-rolling as-received 1 in. diam bar stock by different amounts and recrystallizing the material. Eighty percent cold work followed by heating at 482°F for 2-1/2 hr resulted in an average grain size of about 125μ.

Figure 12 shows the load and unload emission data for 99.99% aluminum for two different average grain sizes, 125μ and about 15μ. Specimen 6(b) showed no unload emission on reloading. Figure 13 shows the dependence of the unload emission on stress for these two different grain sizes.

B. THE EFFECT OF QUENCHED-IN VACANCIES ON THE ACOUSTIC EMISSION BEHAVIOR OF 99.99% ALUMINUM

Two similar specimens of 99.99% Al were heated to 630°C for 2 hr. One specimen was them quenched to -10°C in ice brine, and immediately tested for acoustic emission activity, while the other specimen was allowed to air cool before being tested. The experiment was then repeated with the same two specimens, except that the roles of the two specimens were switched, and the quenched specimen was allowed to age for 3 hr at room temperature. The 3-hr aging treatment enabled the quenched-in vacancies to diffuse through the lattice and form vacancy clusters, or discs. These disc were probably on the order of 200 Å in diam, and spaced about 0.1μ to 0.5μ apart.[13]

20
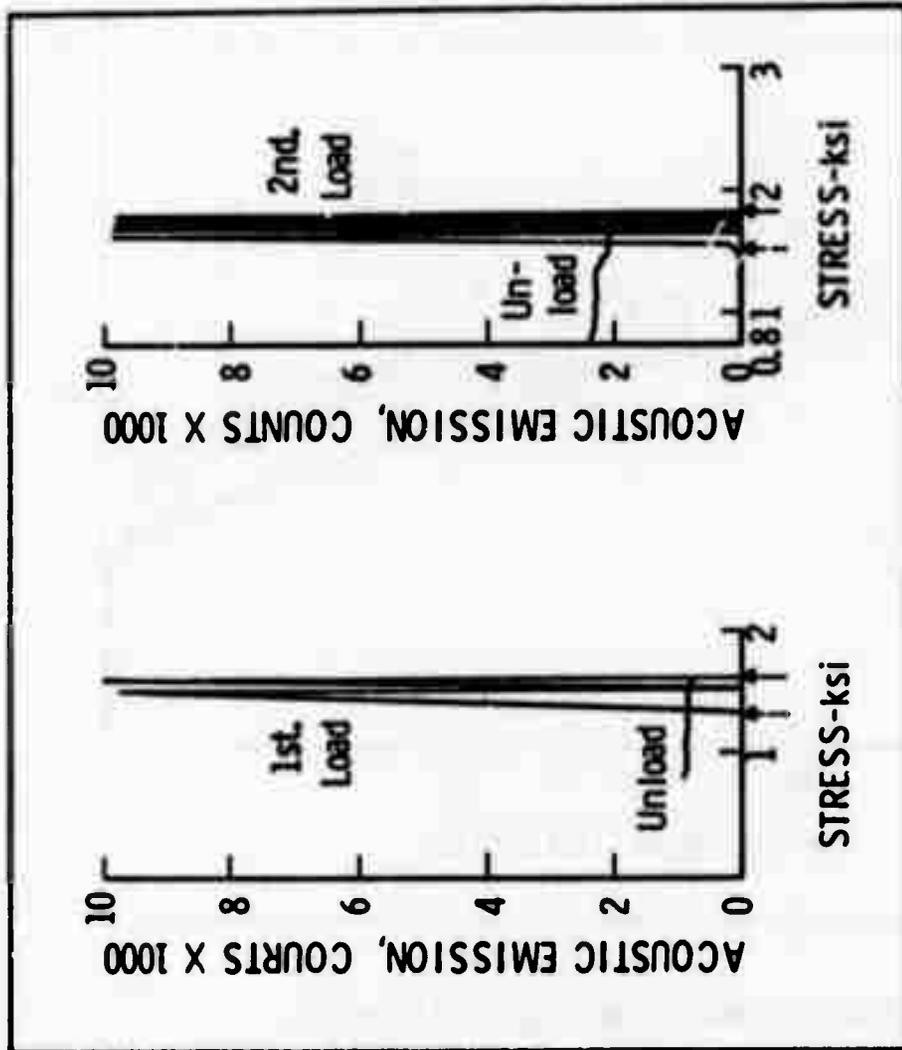
Figure 10. Acoustic emission from a 99.9% aluminum specimen at two different stress levels. The specimen was annealed at 970°F for 3 hr. Average grain size, 1500μ. Hardness, 31 R_H.
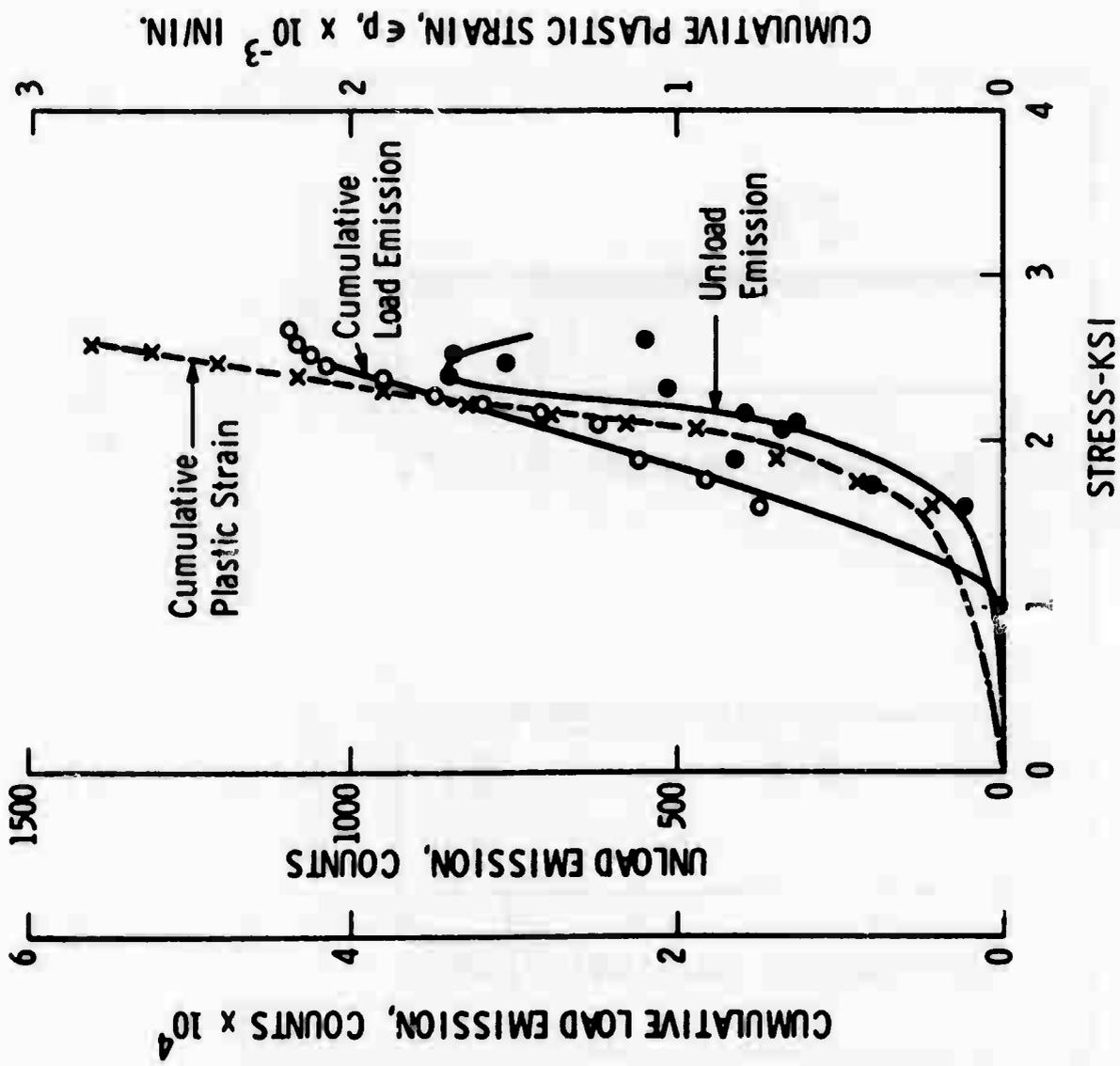
Figure 11. Stress vs. cumulative load emission, unload emission, and cumulative plastic strain in 99.99% aluminum specimen, annealed at 970°F for 3 hr, average grain size, 1500μ, hardness, 31 R_H.
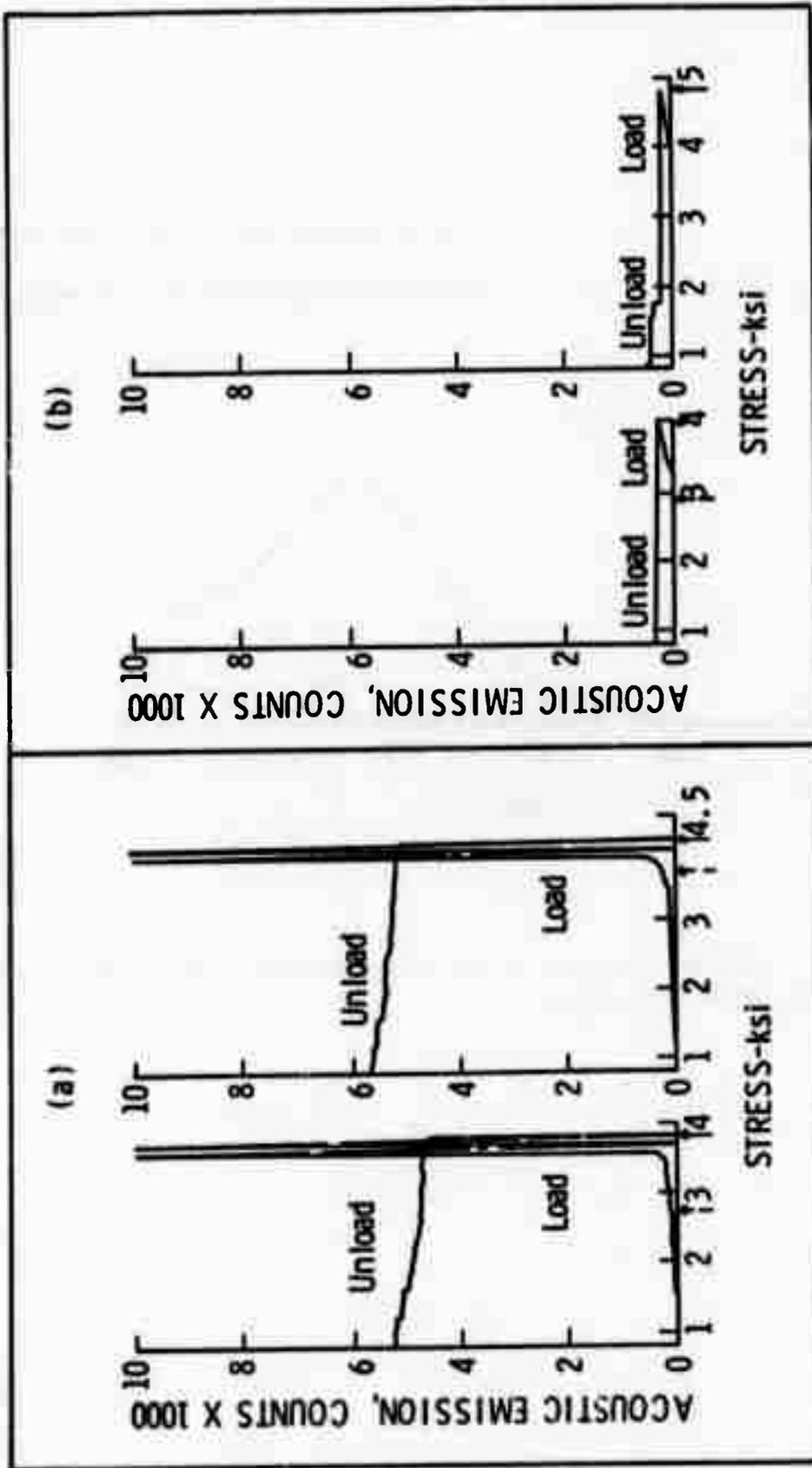
Figure 12. Effect of the grain size on the unload emission of 99.99% aluminum specimens. (a) Acoustic emission from a specimen of average grain size of 125μ. (b) Acoustic emission from a specimen of average grain size of 15μ, at two different stresses.

23
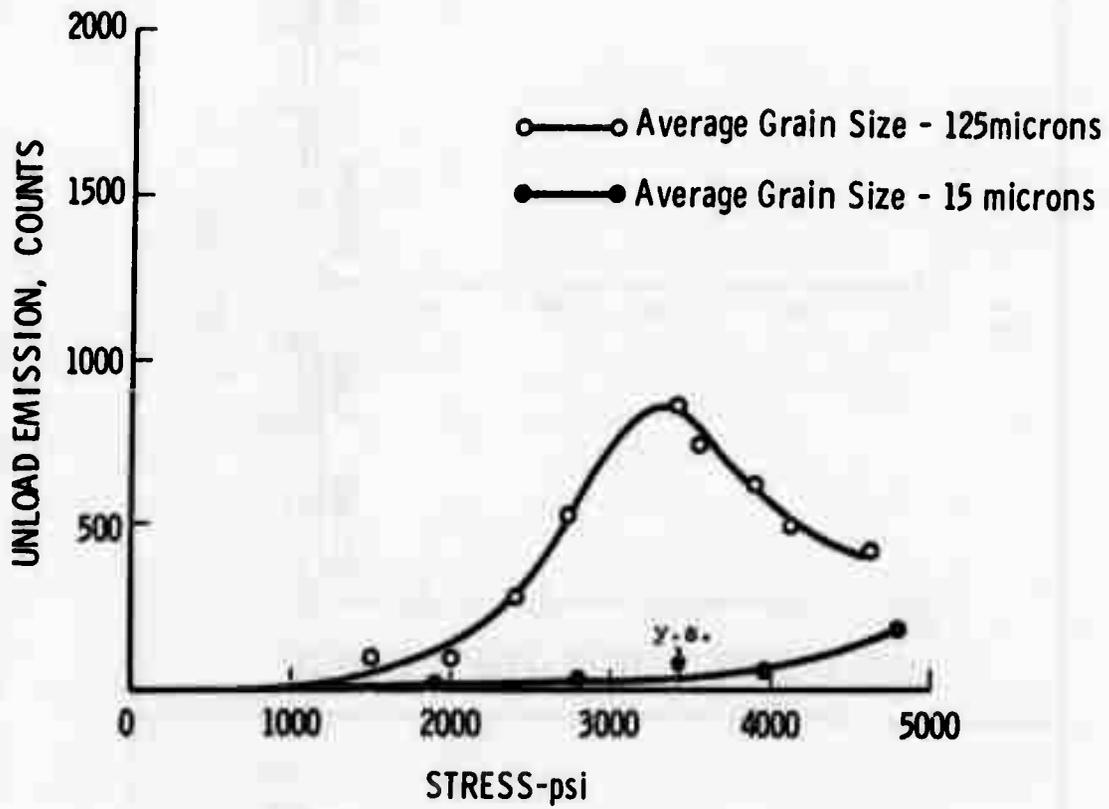
Figure 13. Stress dependence of the unload emission from 99.99% aluminum for two different grain sizes.

The results of the experiment show that the acoustic emission activity is grossly reduced by the presence of quenched-in vacancies because of the pinning effect they have on the dislocations. The presence of discs causes a further reduction in acoustic emission activity. These dislocations effects are clearly observable in Figure 14.

C. ACOUSTIC EMISSION OBSERVED IN 99.99% ALUMINUM DURING LOADING AND UNLOADING

The characteristics of the emission observed varies according to whether subgrains are present in the material or not. In the specimens with 10μ or 20μ subgrains most of the emissions observed are of the isolated "burst" type. The time interval between such bursts is on the order of milliseconds. Long intervals of inactivity, on the order of seconds, are observed in which no bursts at all occur.

In specimens lacking a subgrain structure, the characteristics of the emissions are not observed to depend on grain size. The emission seems to be made up of groups of bursts in which the individual bursts are separated by 10 to 100μ sec. The groups contain 10 to 100 bursts and usually reoccur at a fairly uniform rate. They result in the "steps" in the high-rate-of-emission part of the ΣLE versus applied stress plots, as may be seen in Figure 15. In the intervals between the groups of bursts, a segment of low-rate-of-emission is often observed.

Upon unloading, very little emission is observed. Reloading results in negligible emission until the previously reached load was attained; hence, 99.99% Al displays the Kaiser effect.

1. 0.1 Volt Trigger Level Tests

A series of tests was run with a 0.1 V trigger level setting to determine the effect of grain size on the load emission from 99.99% Al. The results of these tests for a stress of 1500 psi are shown in Figure 16. They show a maximum acoustic emission at a average grain size of about 350μ. The increase in emission with increasing grain size below 350μ is attributed to the increase in the slip distance of the dislocations in the individual grains of the material. The decrease above 350μ is attributed to the decrease in the number of grain boundary sources of dislocation multiplication with the decreasing grain boundary area.

Figure 17(a) shows the variation of cumulative load emission ΣLE with applied tensile stress for cold-rolled specimens of 99.99% Al that have been subjected to a "recovery" heat treatment. They have subgrain sizes of 10μ and 20μ, respectively. The average of the behavior of two specimens of each type is plotted. Note the diminishing rate of emission as the applied stress increases, resulting in a downward concavity of the plots. Similar plots for

(a) as quenched   (b) aged 3 hr   (c) air cooled
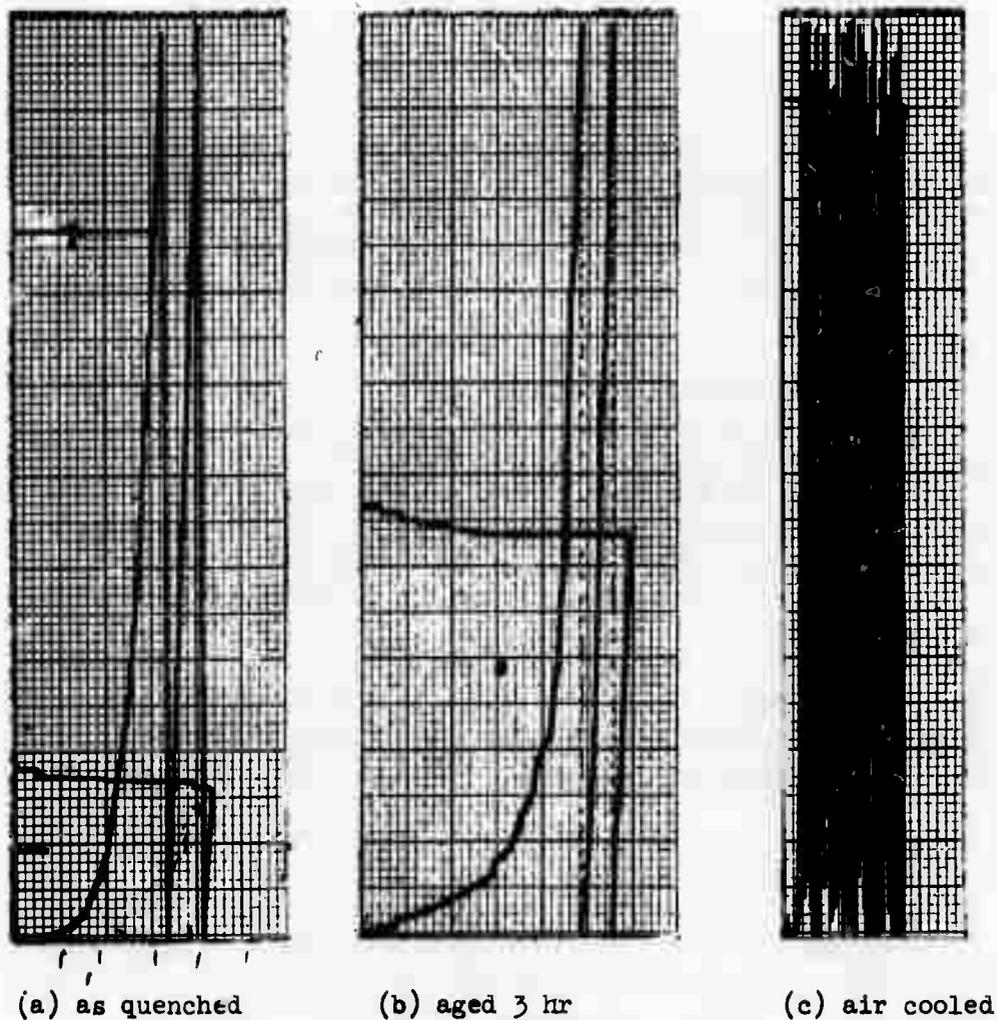
Figure 14. ΣLE vs. applied stress for the acoustic emission from 99.99%
aluminum is diminished by the presence of quenched-in vacancies or vacancy
disks. (a) A specimen which was quenched from 630°C to -10°C, then tested
within 2 min; (b) a specimen which was quenched as in (a), then allowed to
age at room temperature for 3 hr before being tested; (c) a specimen which
was air cooled from 630°C. Each 1/2 in. square on the horizontal scale
represents a 750 psi applied stress increment above a 750 psi preload. The
vertical (ΣLE) scale is 10,000 counts per full scale deflection of the pen,
or 1000 counts per 1/2 in. division. (The frequency range used in these
tests was 8-15 kHz.)
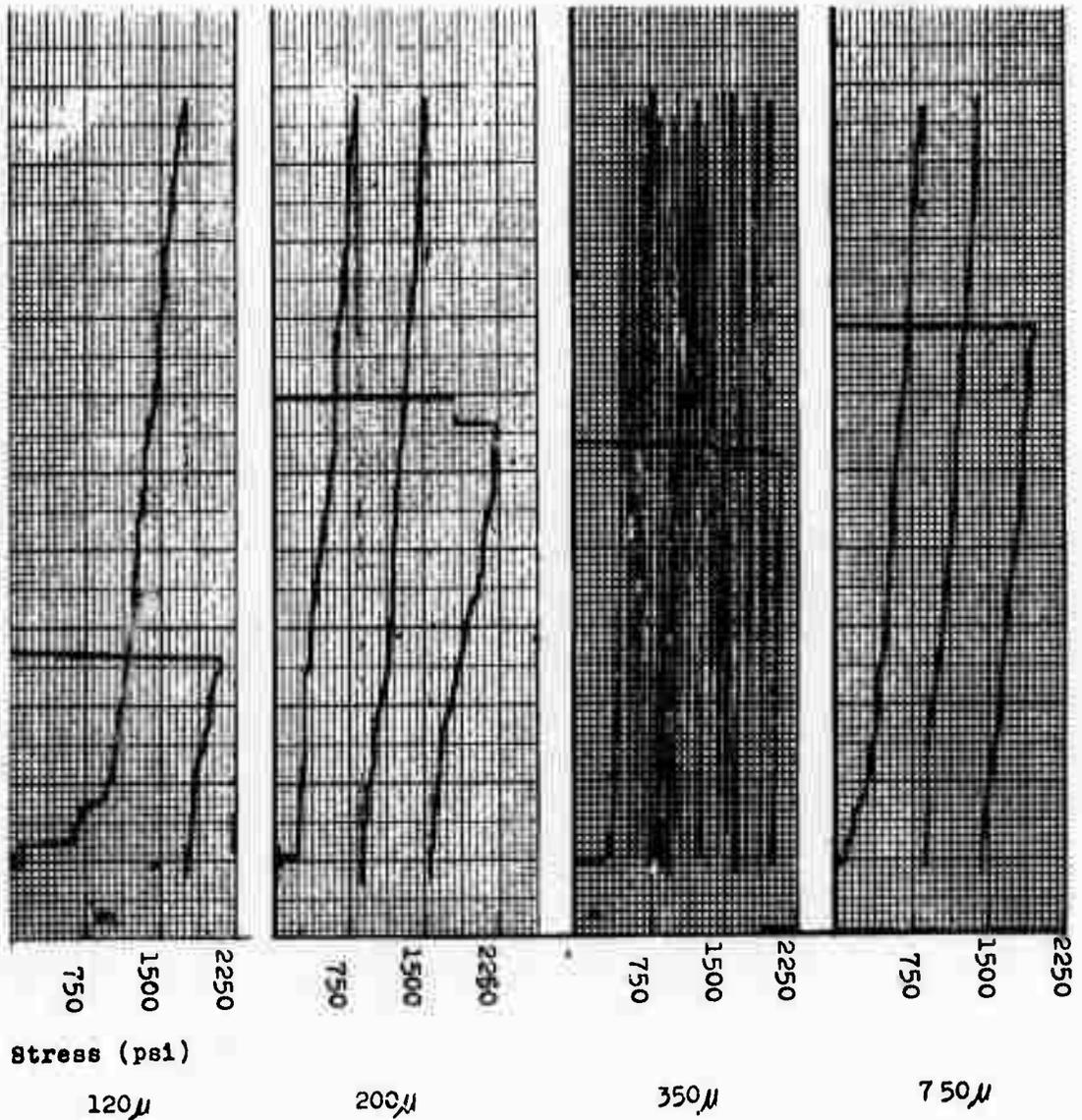
Figure 15. Chart recordings of stress vs. number of counts for four different grain sizes ranging from 120-750μ. The various grain sizes were obtained by the strain-anneal technique. Each 1/2 in. square on the vertical scale is 100 counts. Trigger level is 0.1 V.
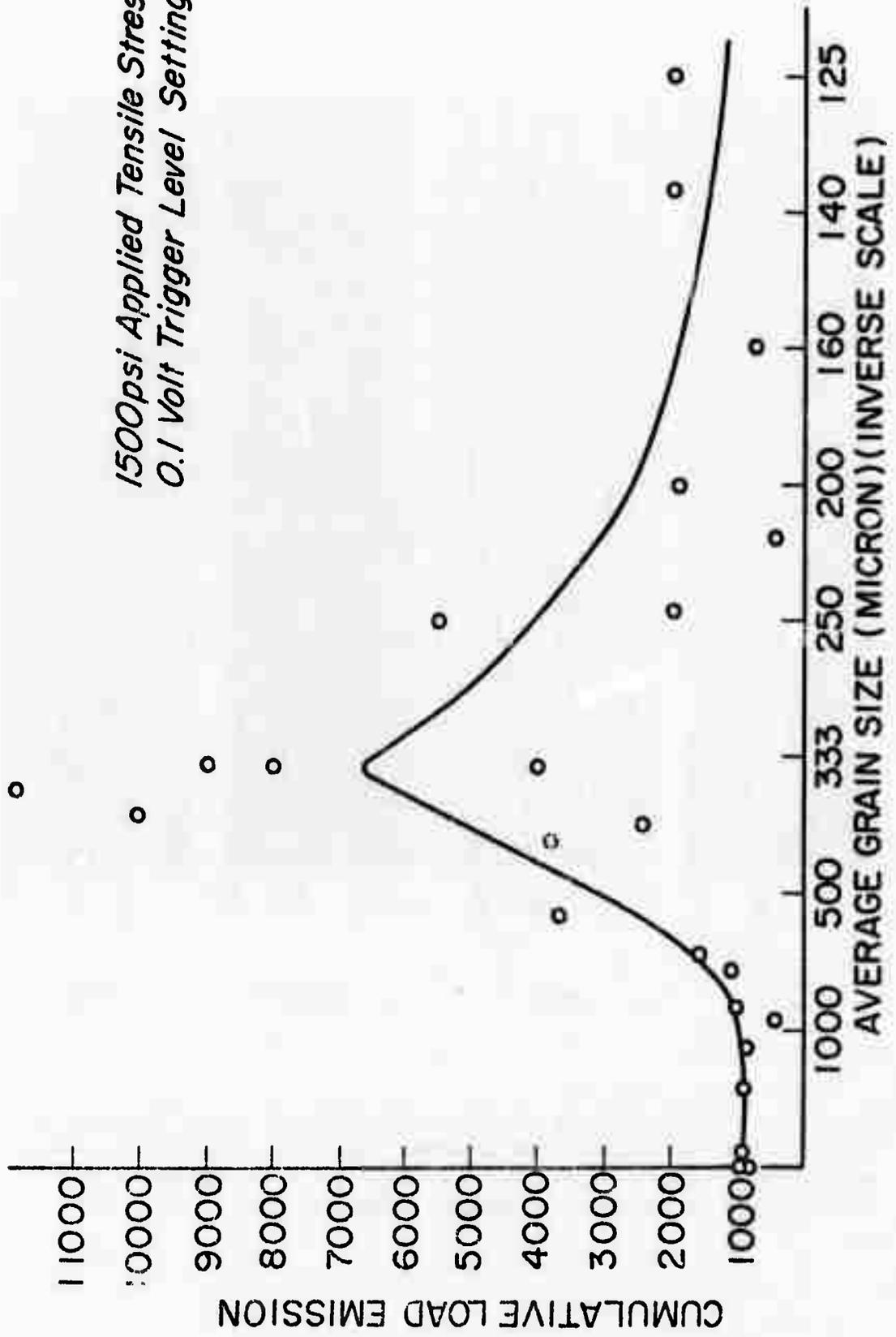
Figure 16. Cumulative load emission vs. grain size for 99.99% Al in the 120-180 kHz bandwidth at 1500 psi with a 0.1 V trigger level setting.

28
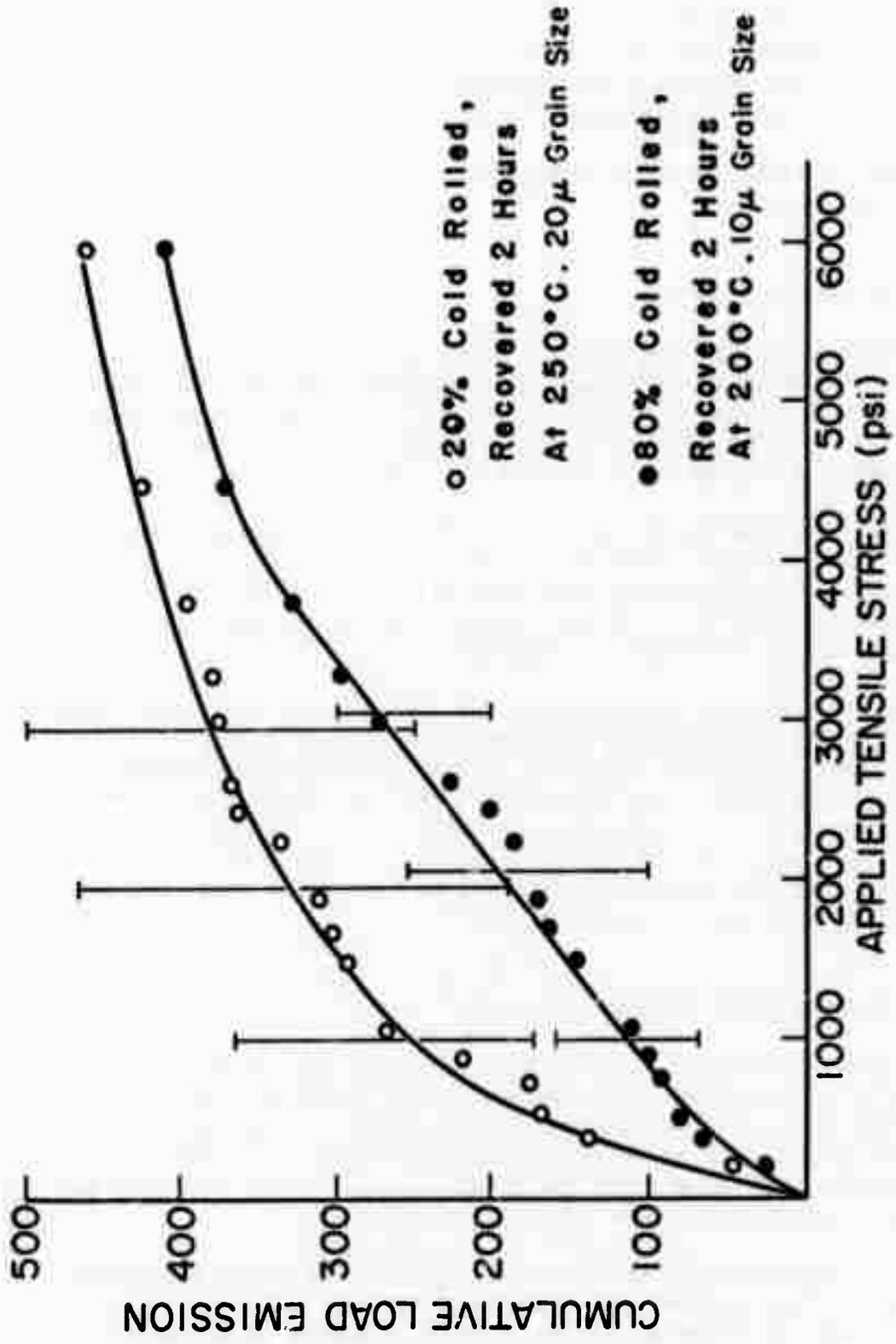
Figure 17(a). Cumulative load emission vs. stress for recovered 99.9% Al.

80% and 20% cold rolled specimens, which were recrystallized to give 650μ and 350μ grain sizes, respectively, are shown in Figure 17(b). The shape of these plots is typical of all recrystallized specimens without a subgrain structure. Figure 17(b) is an average of the data from three specimens of each type. Note the differences in the scales for Figures 17(a,b). The emission from the large grained specimens is about an order of magnitude greater than that from the small grained structures.

2. 0.2 Volt Trigger Level Tests

It was hypothesized that the position of the peak in the ΣLE vs. grain size curve was a function of the trigger level setting of the acoustic emission counter. To test this hypothesis, a series of tests was run with the trigger level set at 0.2 V, rather than 0.1 V, thus doubling the minimum transducer displacement required to register a count on the counter.

Sample chart recorder curves for four different grain sizes are displayed in Figure 18. The scales are identical to those for the 0.1 V trigger level curves. Figure 19 shows ΣLΣ versus grain size at a stress of 1500 psi. Note that the ΣLΣ scale for the 0.2 V trigger level curves is one-tenth that of the 0.1 V trigger level curve shown in Figure 6.

A development of a peak is observed in the 0.2 V trigger level tests which differs in two notable ways from the development of the peak in the 0.1 V trigger level tests. The first difference is that the peak occurs between 400μ and 450μ grain size vs. 333μ for the 0.1 V setting. The second difference is that the height of the 0.2 V trigger level peak is lower relative to the height of the curve away from the peak. For the 0.2 V curve a decline in ΣLΣ with increasing grain size beyond the 450μ peak is very nearly proportional to the reciprocal of the grain diameter $(D)^{-1}$.

D. ACOUSTIC EMISSIONS FROM 99.9% Cu

A more limited investigation was conducted on specimens of 99.9% Cu to see whether a grain size effect was present in the cumulative load emission behavior of this metal. Figure 20 summarizes the results of this series of tests. A peak, the position of which appeared to be stress dependent, occurred at about 150μ grain size for a 10,500 psi tensile stress level. At 13,500 psi, the peak moved to about a 50μ grain size.

There is a significant difference between the emission behavior of 99.9% Cu and 99.99% Al. Test records show that when obtaining cumulative load emission versus applied stress curves for Cu there is a much larger stress increment between emission bursts in 99.9% Cu than in 99.99% Al. This gives the cumulative load emission curves for 99.9% Cu a characteristic "stepped" appearance.
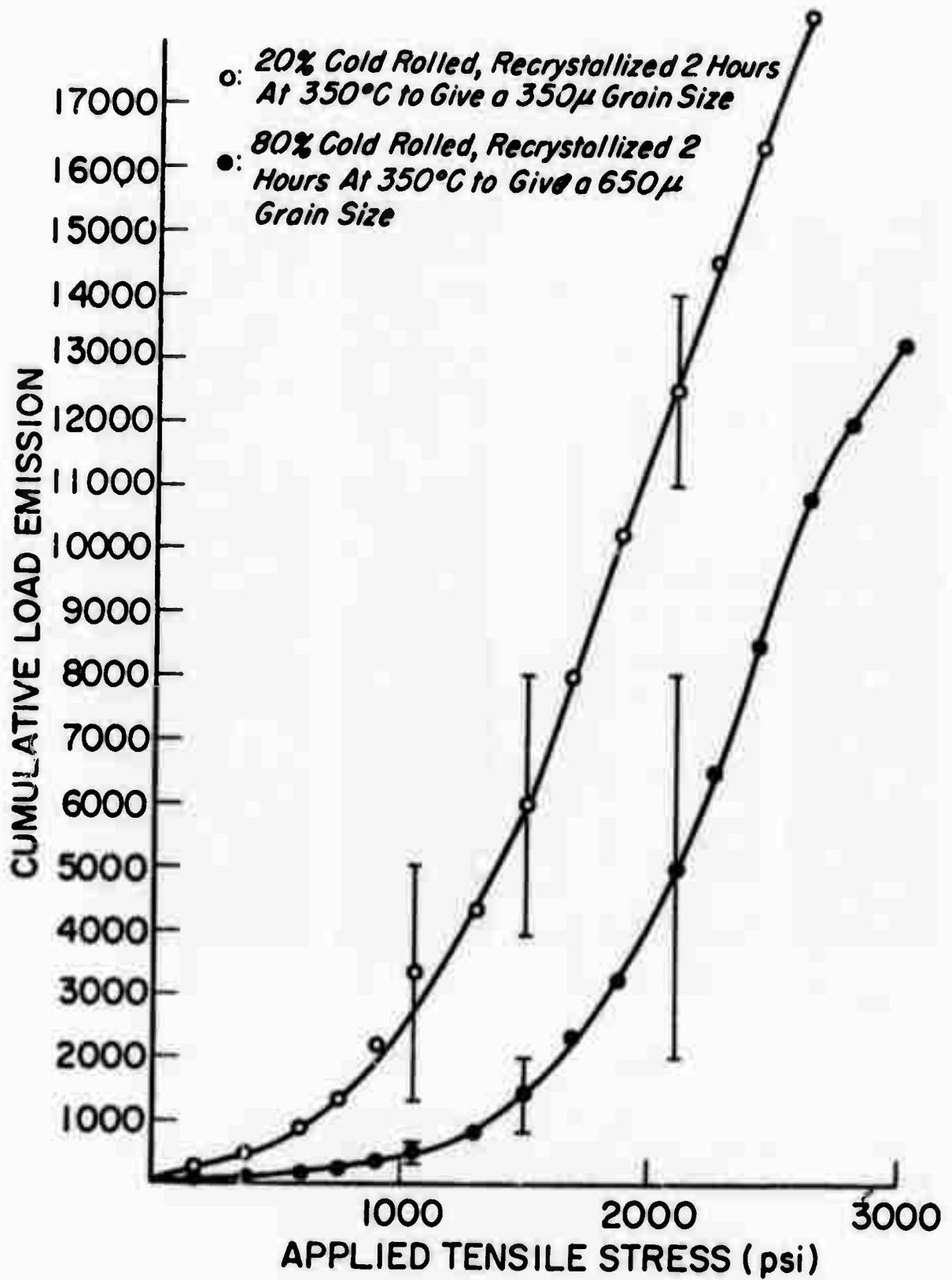
Figure 17(b). Cumulative load emission vs. stress for recrystallized
99.99% Al specimens.

31
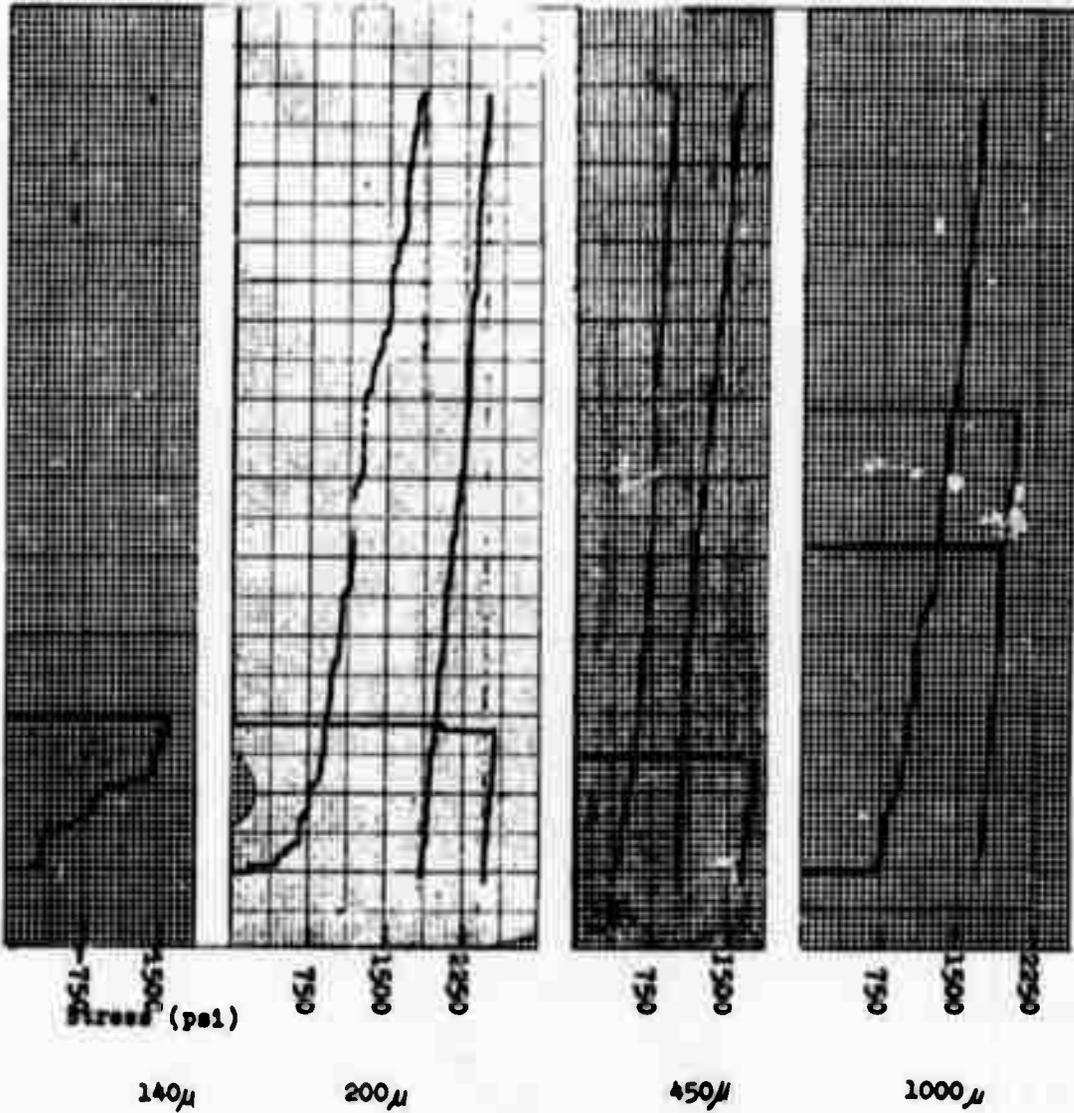
Figure 18. Chart recordings of number of counts vs. stress for four different grain sizes. Each 1/2 in. square on the vertical scale is 100 counts. Trigger level is 0.2 V.
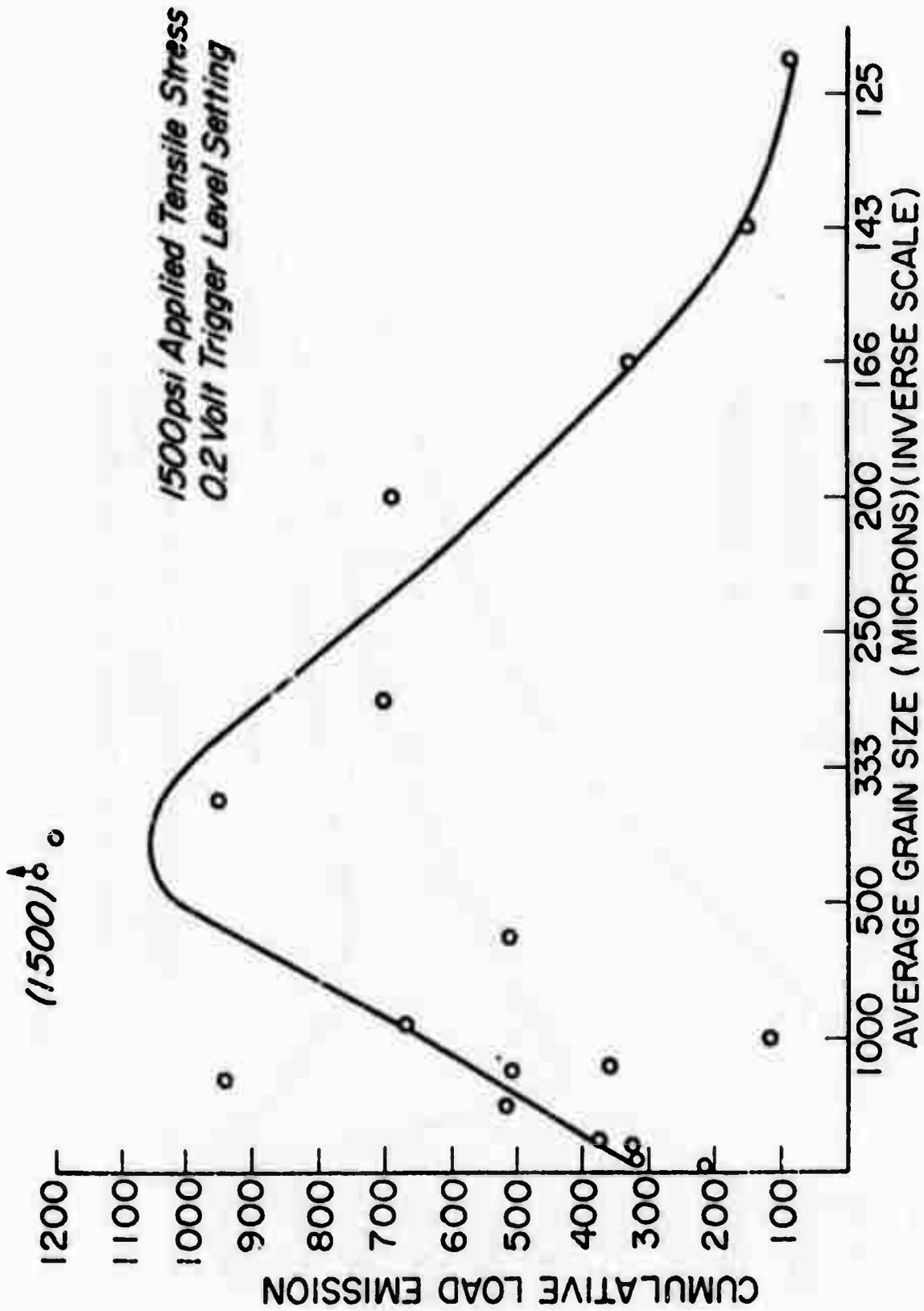
Figure 19. Cumulative load emission vs. grain size for 99.99% Al in the 120-150 kHz bandwidth at 1500 psi with a 0.2 V trigger level setting.

33
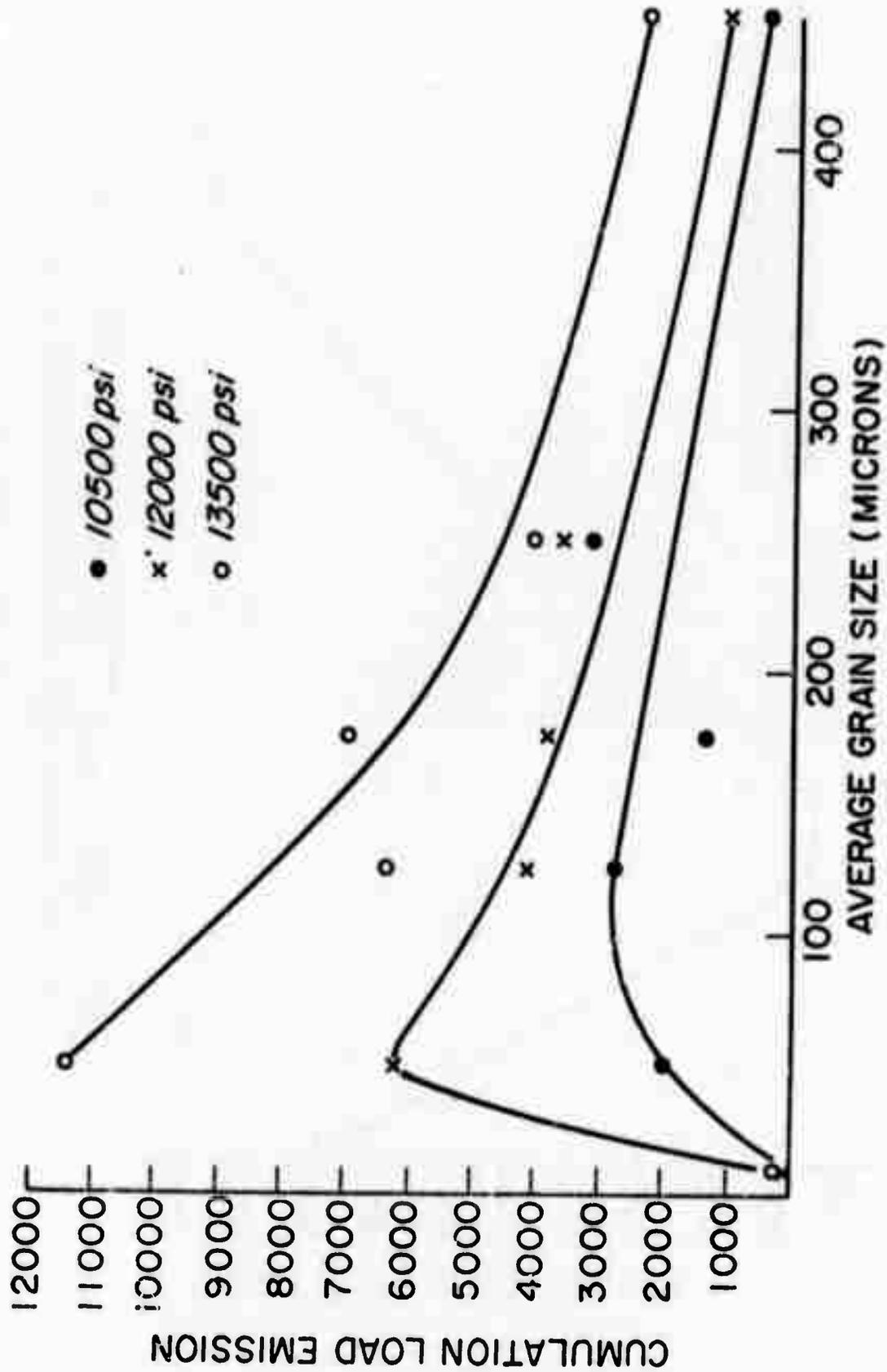
Figure 20. Cumulative load emission vs. grain size for 99.99% Cu.

The emission from both the Cu and the Al occurs in successive groups of bursts. The magnitude of each burst in Cu is large at the beginning of a group, with the signal height declining almost linearly with time. The linear decline in magnitude is in contrast to a fairly uniform magnitude which is seen in groups of bursts from 99.99% Al. The bursts from 99.9% Cu are 5 to 10μ sec apart, and a typical group of 20 to 40 bursts lasts about 200μ sec, compared to 400 or 500μ sec for 99.99% Al. This group-of-bursts quality probably results from a situation in the grains of the metal in which a localized slip event occurs, relaxing stresses in a region of the specimen. This highly local relaxation of stresses triggers other slip events in neighboring regions, resulting in a series of microstrain events occurring in a very short time interval, and within a small volume of the specimen. Stress concentrations resulting from dislocation pile-ups associated with the microstrain event may also play a role in the triggering of a series of events.

E. LOAD AND UNLOAD EMISSION BEHAVIOR OF VARIOUS MATERIALS

Figure 21 shows stress vs. strain, load emission, and unload emission curves for annealed 6061 aluminum alloy. Figure 22 shows load and unload emission curves for annealed 2024 aluminum alloy. Similar curves are obtained for the following annealed materials: 70-30 brass, a Cu-7.9% Al alloy, 99.95% magnesium, and 99.99% aluminum, except that they differ quantitatively.[32] Figure 23 summarizes the unload emission data for the above materials. The results are plotted vs. plastic strain because of the greater significance of strain as far as dislocation motion is concerned. The scatter in the data for the Cu-7.9 Al alloy is because of the relatively low strain. Data at higher stress levels do lie on an extension of the curve.

Tests were conducted on 6061 alloy with different aging treatments in order to observe the effect of hardness on the unload emission. Five identical specimens were solution treated by heating at 970°F for 3 hours. Aging was done at 400°F for different lengths of time. The resulting hardness values are shown in Table II. All the specimens were subjected to a maximum stress of 6600 psi in one load-unload cycle. Figure 24 shows the effect of hardness on unload emission for the differently heat-treated specimens.

F. CORRELATION BETWEEN THE OBSERVED UNLOAD EMISSION AND THE MAGNITUDE OF THE BAUSCHINGER EFFECT

An effort was made to determine if a correlation exists between the unload emission of 2024 aluminum alloy with different aging treatments and the corresponding Bauschinger effect. Four speciments of 2024 aluminum alloy were solution treated by heating at 970°F for 3 hr. The aging treatments and the hardnesses attained are shown in Table III. All the specimens were subjected to a maximum stress of 8250 psi in one load-unload cycle. Table III also shows the emission response. As aging progresses, acoustic emission decreases, goes though a minimum value and then increases.
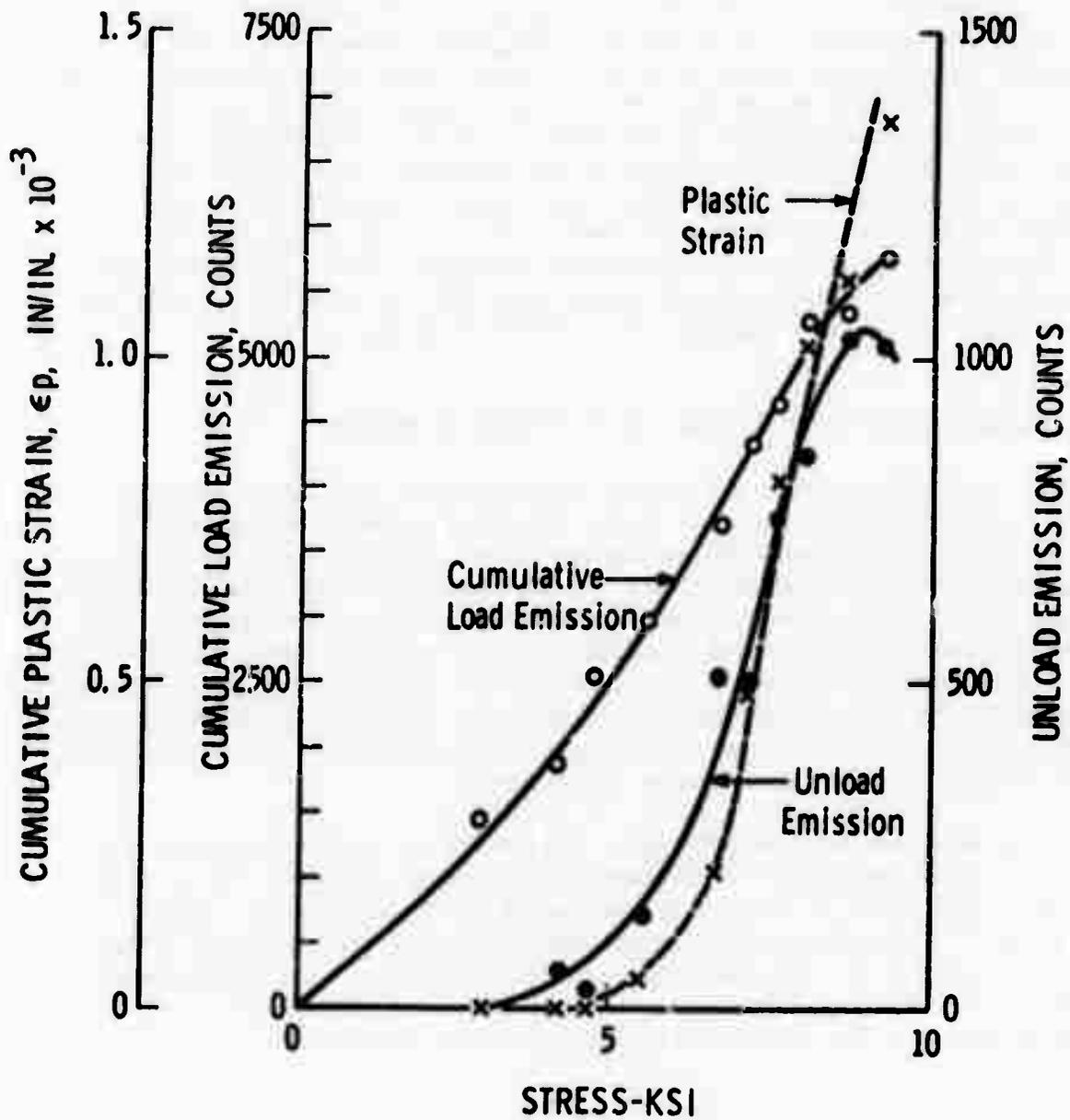
Figure 21. Stress vs. cumulative load emission, unload emission, and cumulative plastic strain in a 6061 aluminum alloy specimen, annealed at 970°F for 3 hr. Average grain size 55µ; hardness 15 R_E.
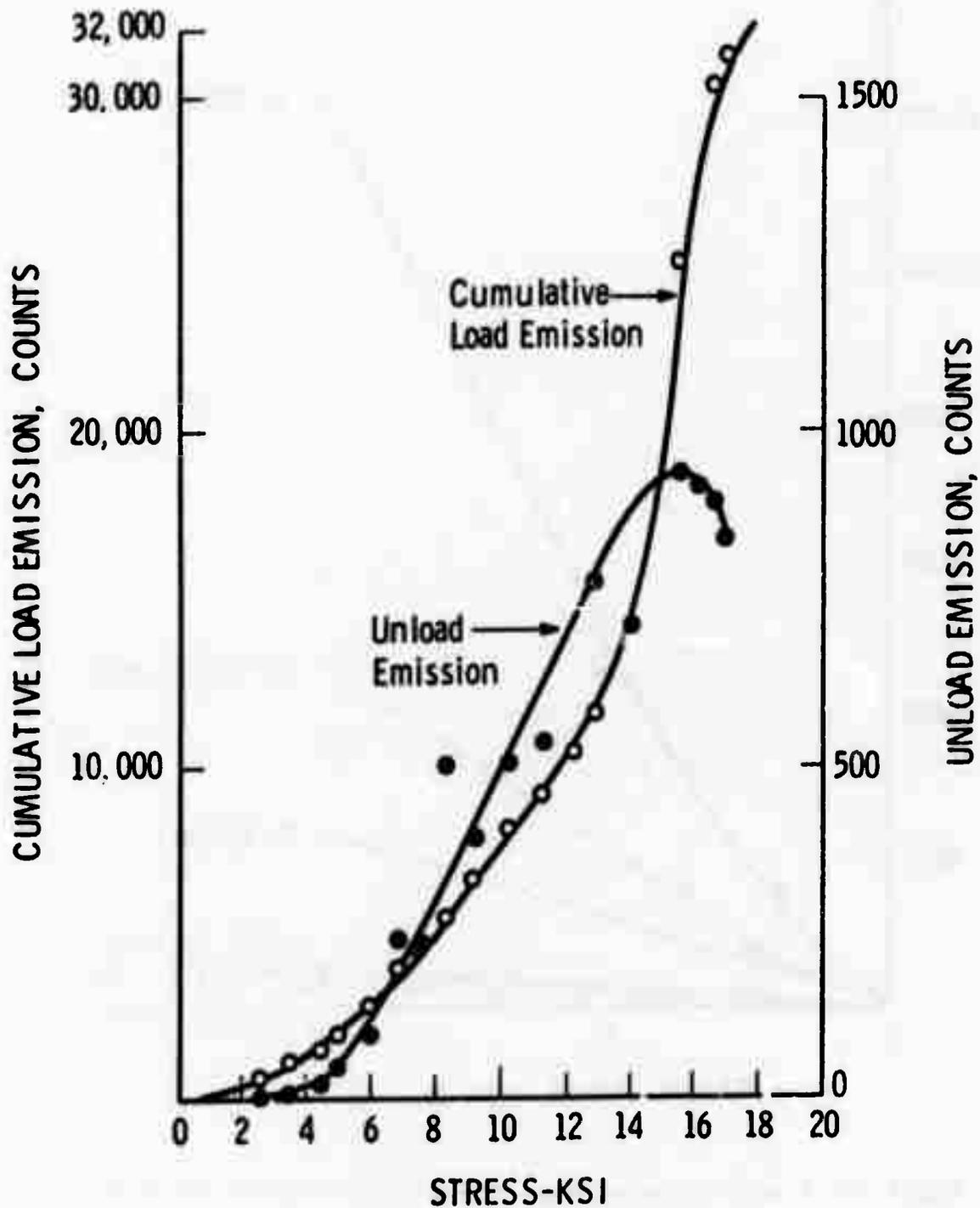
Figure 22. Stress vs. cumulative load emission, and unload emission in a 2024 aluminum alloy specimen, annealed at 970°F for 3 hr. Average grain size 110μ; hardness 65 R_E.
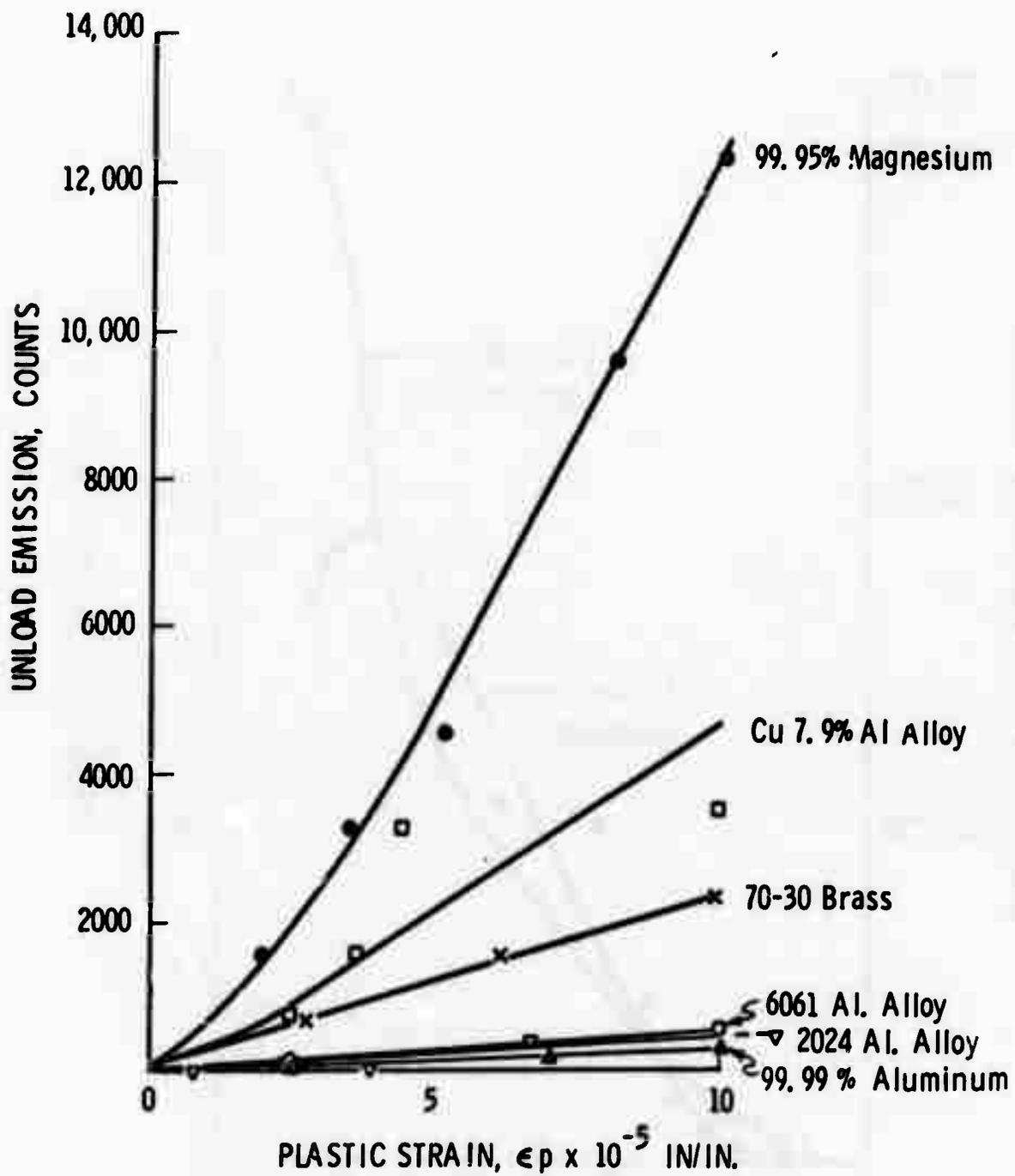
Figure 23.   Strain vs. unload emission for certain annealed materials.
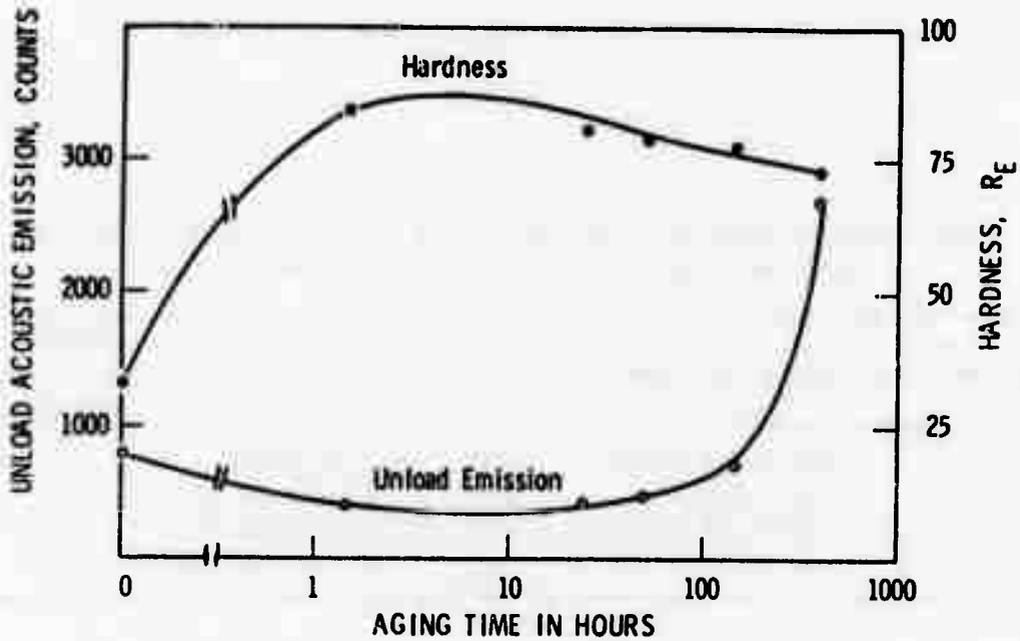
Figure 24. Aging time vs. unload emission and hardness for 6061 aluminum alloy specimens. The specimens were aged at 400°F for different periods of time. All the specimens were subjected to a maximum stress of 6600 psi.

TABLE II

AGING TIME AND RESULTANT HARDNESS OF 6061 ALUMINUM ALLOY

Specimen No.	Aging Time at 400°F in hr	Hardness, R_E
81	0	36
82	1.5	94
84	24	87
85	49	84
86	144	82
87	373	72

TABLE III

AGE-HARDENING TREATMENT, HARDNESS, THE RESULTANT MICROSTRUCTURE, AND THE UNLOAD EMISSION IN 2024 ALUMINUM ALLOY

Specimen No.	Aging Treatment	Hardness, R_E	Microstructure	Unload Emission, Counts
71	264°F for 16 hr	100	G-P zones	697
72	320°F for 5 hr	103	θ'' precipitate	562
73	428°F for 5 hr	101	θ' precipitate	621
74	572°F for 5 hr	91	θ preciptiate	715

Table IV shows the microstructure dependence of two measures of the Bauschinger effect, the Bauschinger strain, and the Bauschinger stress, with the unload emission for the same specimens listed in Table III. The unload emission correlates with the Bauschinger stress, but not the Bauschinger strain.

The Bauschinger strain was measured for several annealed materials. The results are shown in Table V along with the unload emission and the stacking fault energy for various materials. It can be seen that low values of unload emission correspond to low values of Bauschinger strain and high values of the stacking fault energy. The unload emission correlates well with Bauschinger strain, except for an inversion in order by 2024 and 6061 aluminum. Large values of unload emission correlate with large values of Bauschinger strain and low values of stacking fault energy.

TABLE IV

BAUSCHINGER EFFECT AND UNLOAD EMISSION IN 2024 ALUMINUM ALLOY
HEAT TREATED TO GIVE DIFFERENT MICROSTRUCTURES

Heat Treatment	Microstructure	Unload Emission	Bauschinger Strain,* μ in./in.	Percentage Bauschinger Stress**
Aged at 264°F for 16 hr	G-P zones	697	90	44
Aged at 320°F for 5 hr	θ" precipitate	562	90	14
Aged at 428°F for 5 hr	θ' precipitate	621	1120	16
Aged at 572°F for 5 hr	θ precipitate	715	2080	61

*The Bauschinger strain is calculated at a compressive stress which is 50% of the
tensile stress needed to obtain a strain of 0.001 in./in.
**Percentage Bauschinger stress is defined as $\sigma - \sigma_c/\sigma$. σ is the highest stress in
tensile loading and σ_c = stress to initiate yield in reversed loading. The
values of σ and σ_c are taken from Abel and Ham.(13)

41

TABLE V

STACKING FAULT ENERGY, BAUSCHINGER EFFECT, AND
UNLOAD EMISSION IN SEVERAL ANNEALED MATERIALS

Material	Crystal Structure	Stacking Fault Energy, ergs/cm^2	Bauschinger Strain, μ in./in.*	Unload Emission, Counts**
99.99% aluminum	fcc	200	100	340
6061 aluminum alloy	fcc	117	480	610
2024 aluminum alloy	fcc	---	510	580
70-30 brass	fcc	10-12	1150	2400
Cu-7 9% aluminum alloy	fcc	4	1210	4700
99.99% magnesium	hcp	---	3000	12400

*Bauschinger strain was measured at a compressive stress which was 50% of the tensile stress
  needed to produce a strain of 0.005 in./in.

**Unload emission counts were recorded for a cumulative plastic strain of 0.0001 in./in.

G. RESIDUAL STRESS TEST RESULTS

The results of the acoustic emission tests on an annealed (stress-free) and the residual stress specimens are shown in Figures 25-28. The curves shown are reproducible to within ±3% on any particular specimen. A preload of 50 lb was maintained on the specimens when making a test, hence the applied load is shown in the figures as ranging from 50 to 400 lb. The maximum load of 400 lb in all tests is less than half the yield stress of the materials.

The effect of residual compressive stresses on the acoustic emission from the 6061-T6 aluminum specimen that has been bent about 1/2° and restraightened is evident by comparing Figures 25(a) and 25(b). The emission obtained on loading the specimen is greater than when no residual compressive stresses are present and there is an increasing rate of emission on loading up to the stress at which the compressive stress is overcome by the applied tensile stress. This point is indicated by the arrow on the graph at a load of about 250 lb. Beyond this load the rate of increase of emission is constant.

According to the model described in Figure 7 there should be a point of inflection on the unload part of the curve. This is not evident, however, perhaps because of the low value of the unload stress that is associated with that part of the specimen having residual compressive stress.

Figure 26 shows the emission from a 1018 flat steel specimen having no residual stresses. The constant rate of emission obtained on the application of a load can be noted. In Figures 27 and 28, however, the emission rate increased during the application of a load. In both specimens it is evident that the applied stress was not sufficient to overcome the residual compressive stress and there is no inflection point on the load curve.

H. CREEP TEST RESULTS

Figure 29 shows the results of the creep tests carried out at room temperature on a specimen of 99.99% aluminum.

Excessively high background noise levels made it impossible to obtain significant results on the 7075-T6 aluminum, D6aC steel, or the 6Al-4V titanium at elevated temperatures.

I. THERMAL STRESS RESULTS

The thermal stress tests were primarily qualitative because of the difficulty in knowing the magnitude of the stress levels that were produced or the distribution of the stresses that result from bubble formation.

It was found that all of the methods used for producing thermal stresses were able to produce acoustic emission in specimens that would normally be ex-
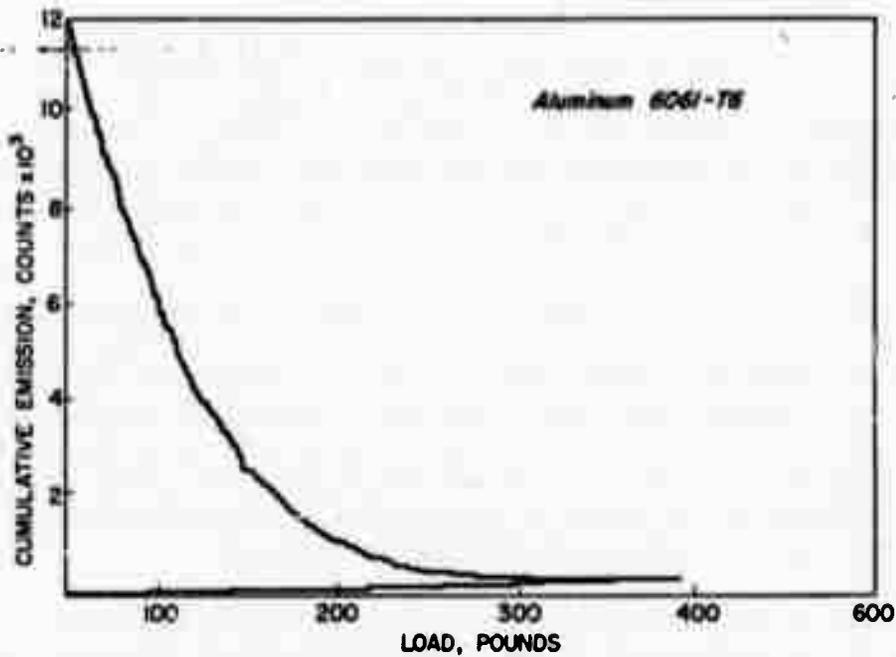
Figure 25(a). Cumulative acoustic emission from 6061-T6 aluminum during loading and unloading. The maximum stress applied to the specimen is less than half of the yield stress.
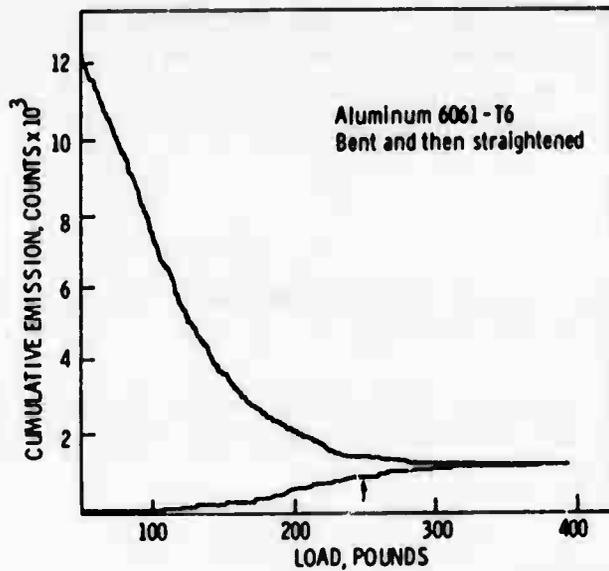
Figure 25(b). Cumulative acoustic emission from a 6061-T6 aluminum specimen that had been bent to about 1/2° and then restraightened. The arrow indicates a region of the load curve in which there is a change in slope, as might be expected from the model in Figure 7. The applied stress is less than half the yield stress.
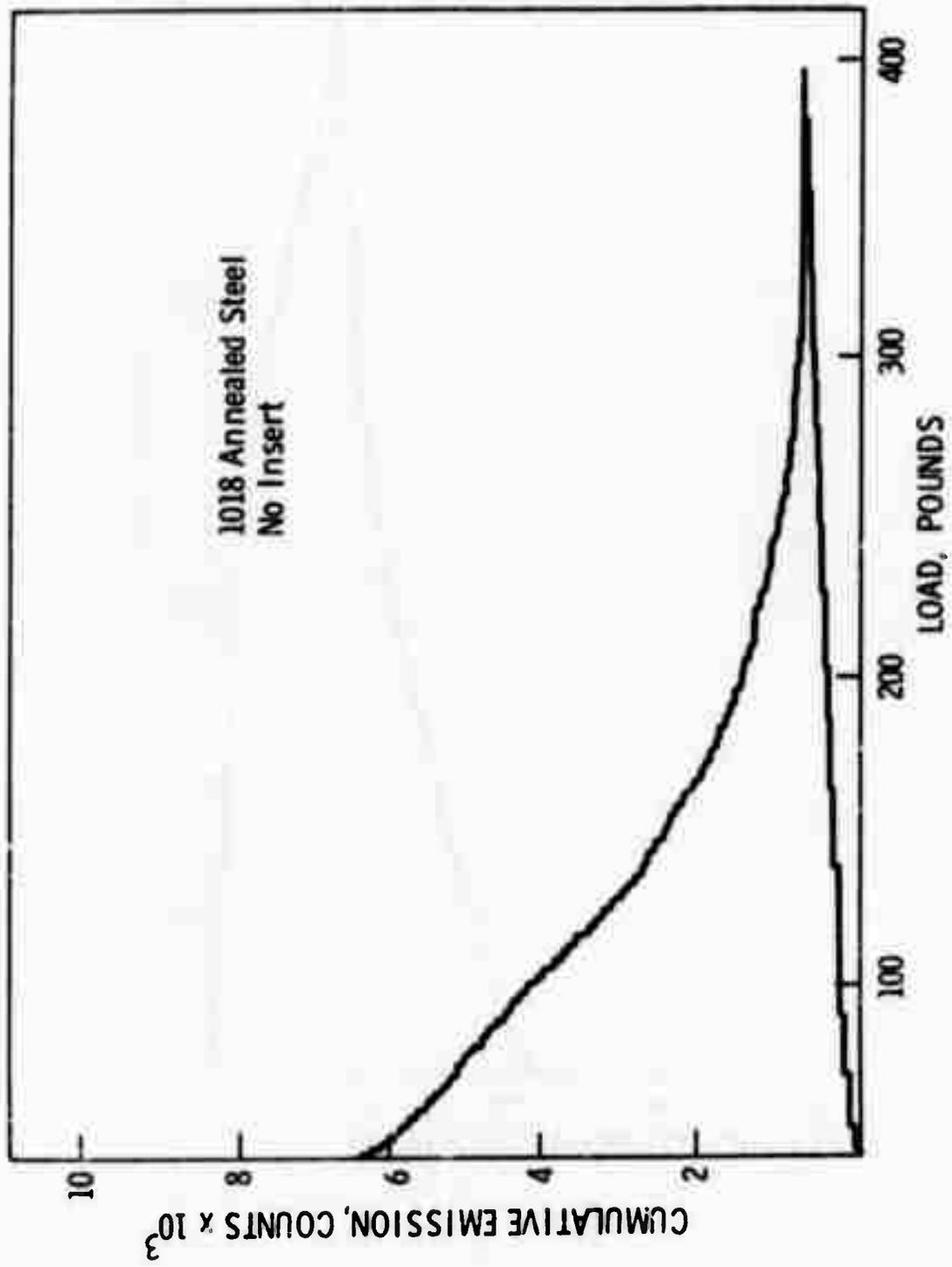
Figure 26. Acoustic emission from an annealed 1018 steel flat tensile specimen which has no residual stresses.

45
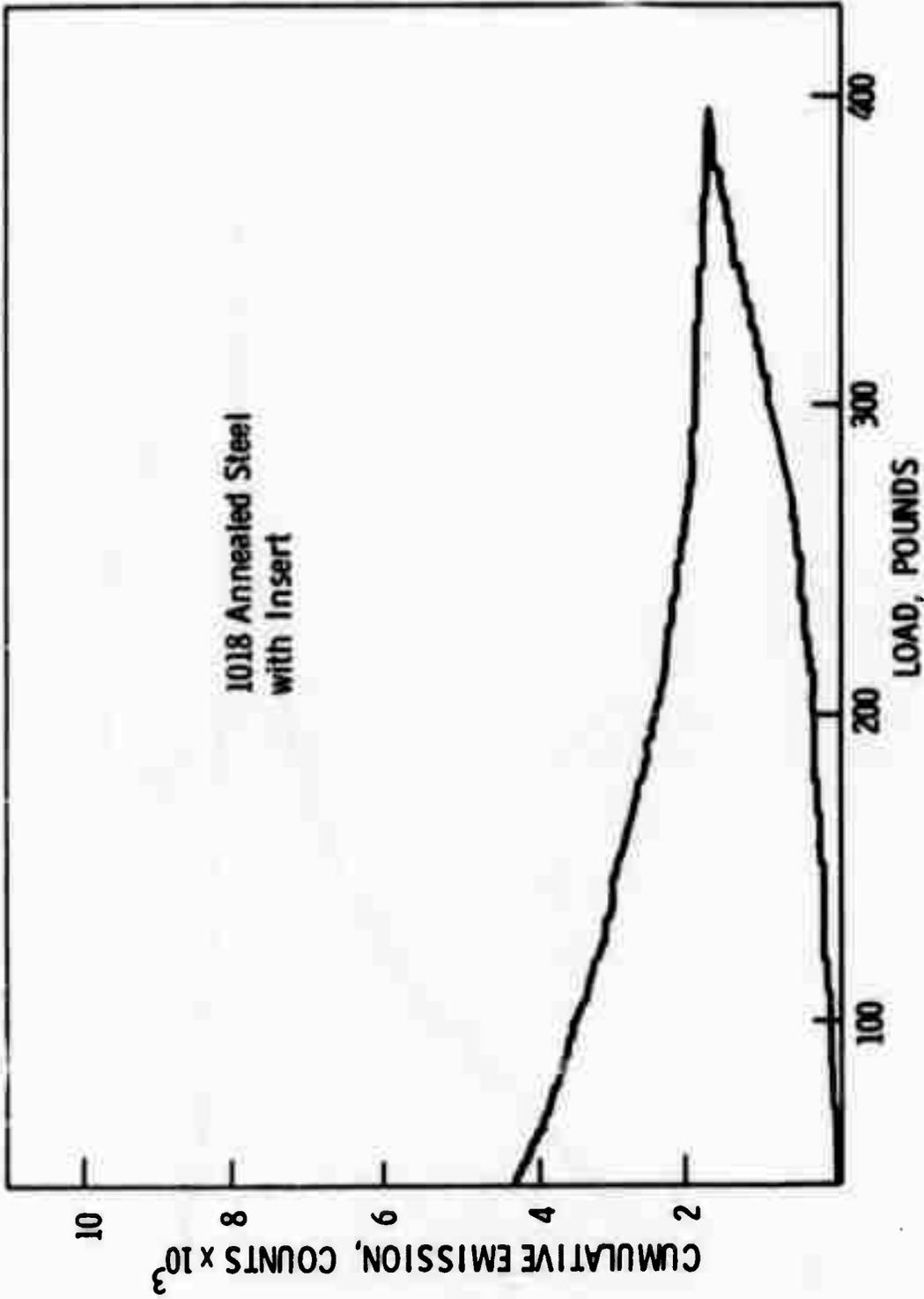
Figure 27. Acoustic emission from an annealed 1018 steel flat tensile specimen containing a shrunk-fit insert having a compressive stress of about 16,000 psi.

46
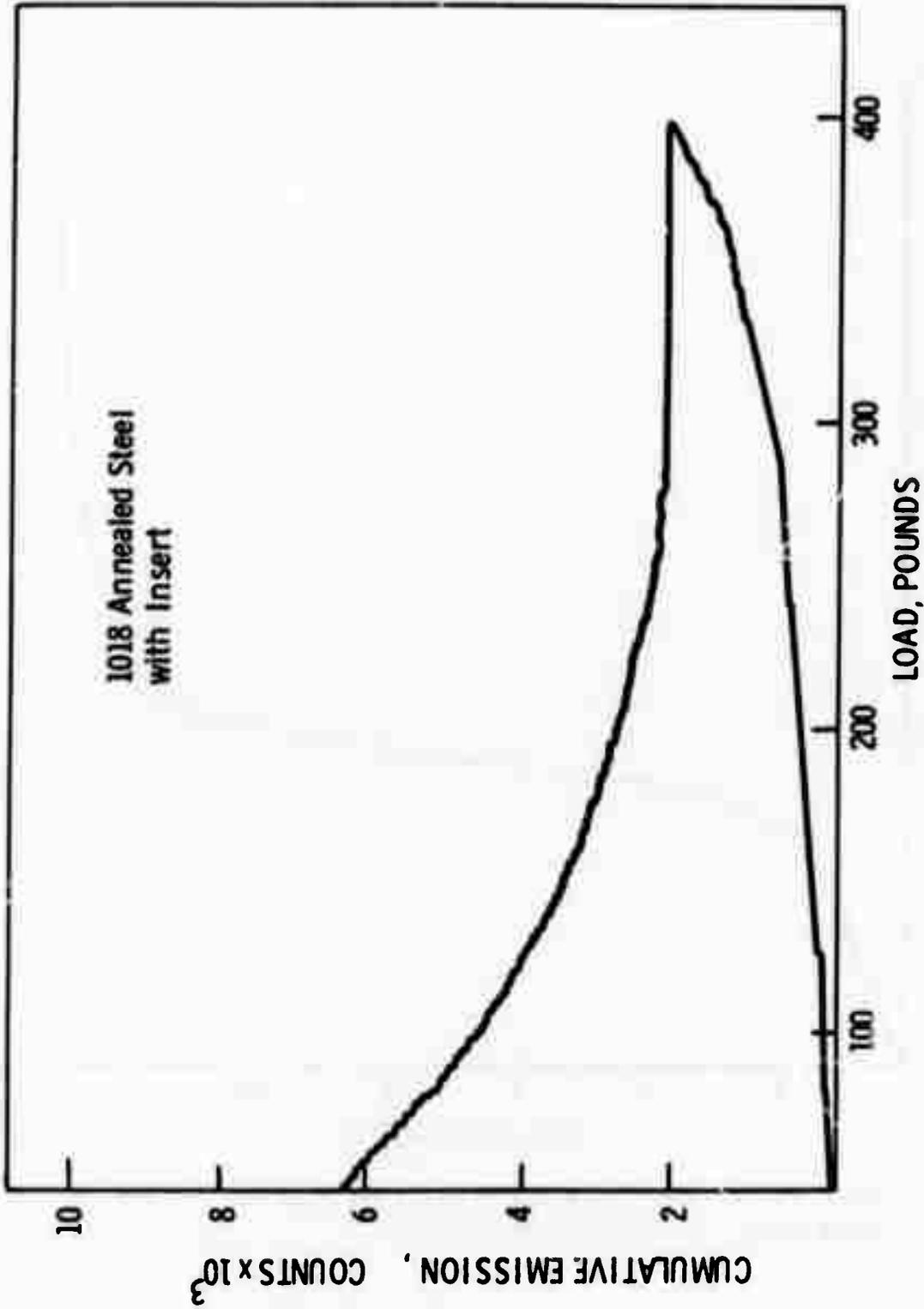
Figure 28. Acoustic emission from an annealed 1018 steel flat tensile specimen containing a rolled-in insert having a compressive stress of about 6000 psi.

47
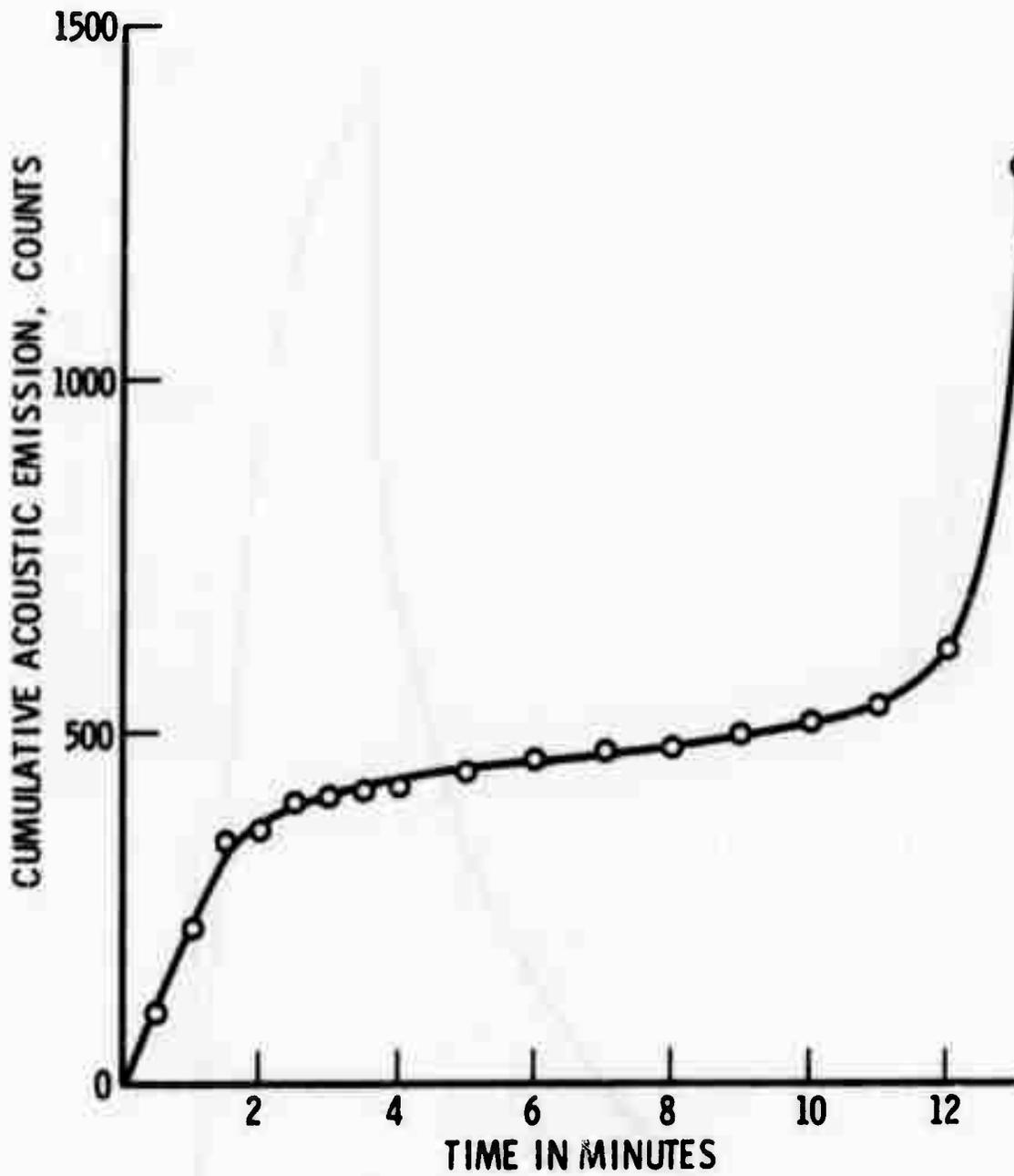
Figure 29.   Acoustic emission from 99.99% aluminum
during creep.   Initial stress 9400 psi.

expected to give off emission if stressed. However, the usefulness of liquid nitrogen as a means of cooling is limited by the high noise levels.

The principal requirement is that the rate of heating (or cooling) is sufficient to produe a thermal stress gradient. This means, for example, that on metals it is necessary to use an intense laser beam source, or a quench technique because of the relatively high thermal conductivity. On polymers, an infrared source is sufficient because of their lower thermal conductivity.

V. DISCUSSION OF RESULTS

A. APPLICATION OF THE DISLOCATION SOURCE MODEL TO TEST RESULTS

Annealed 99.99% aluminum: The high values of acoustic emission that have been measured for this material indicate the presence of sources greater than 0.5μ in length, in fact probably of the order of 10-100μ. This is also the range of the size of cell and subcell structures observed in electron-microscope pictures of this material. The region of detectable emission shown in Figure 1 for source lengths of 0.5-100μ shows that a wide range of L/f, where L is the slip region diameter and f is the dislocation source length, can be expected to give measurable emission. Both air-cooled and furnace-cooled specimens of this material give detectable emission. This suggests that even if the impurities have some pinning effect, the source lengths that are encountered are still large enough to be detected. Tests on 2024 aluminum also show that water quenching from 975°F (524°C) results in large load emission but air- and furnace-cooling from the same temperature apparently allow enough precipitation of impurities to prevent detectable load emission for occurring. Subsequent over-aging causes the emission to return slightly.

Cold-worked 99.99% aluminum: If it is assumed, for purposes of a rough calculation, that the increase in dislocation density as a result of cold-work produce a uniform simple cubic network of progressively smaller unit size, it is possible to make an estimate of the highest dislocation density for which acoustic emission can be detected in these tests. A reasonable value of L/f for such a network may be taken as 3. Figure 1 gives the minimum detectable source length for this condition as about 12μ, the intercept of the $L = 3f$, $n = 2$ line with the threshold line. Since the dislocation density found in annealed material is about 10^5 to 10^6 lines per sq cm very little strain hardening is required to reduce the source length to less than 12μ and eliminate detectable load emission. This has been observed in all tests conducted to date, even when the test loading is not in the same orientation as the cold-work deformation loading.

Naturally-aged 2024 aluminum: As the precipitates form gradually following solution heat treating, the maximum value of the dislocation source length f decreases until it is less than 0.25μ. Alloys of this composition are known to have an average particle spacing[15] in the range 0.015-0.050μ. If f is of the same order of magnitude as the particle spacing, then Figure 1 indicates that no emission should be detectable from a fully aged 2024 aluminum alloy. The fine cross-hatched region for 2024-T4 does, in fact, fall well below the threshold curve. Partially aged 2024 should give a limited amount of detectable emission because the particles would be expected to have average spacing in the micron range. This agrees with the experimental results obtained by Agarwal[6] as shown in Figure 30.
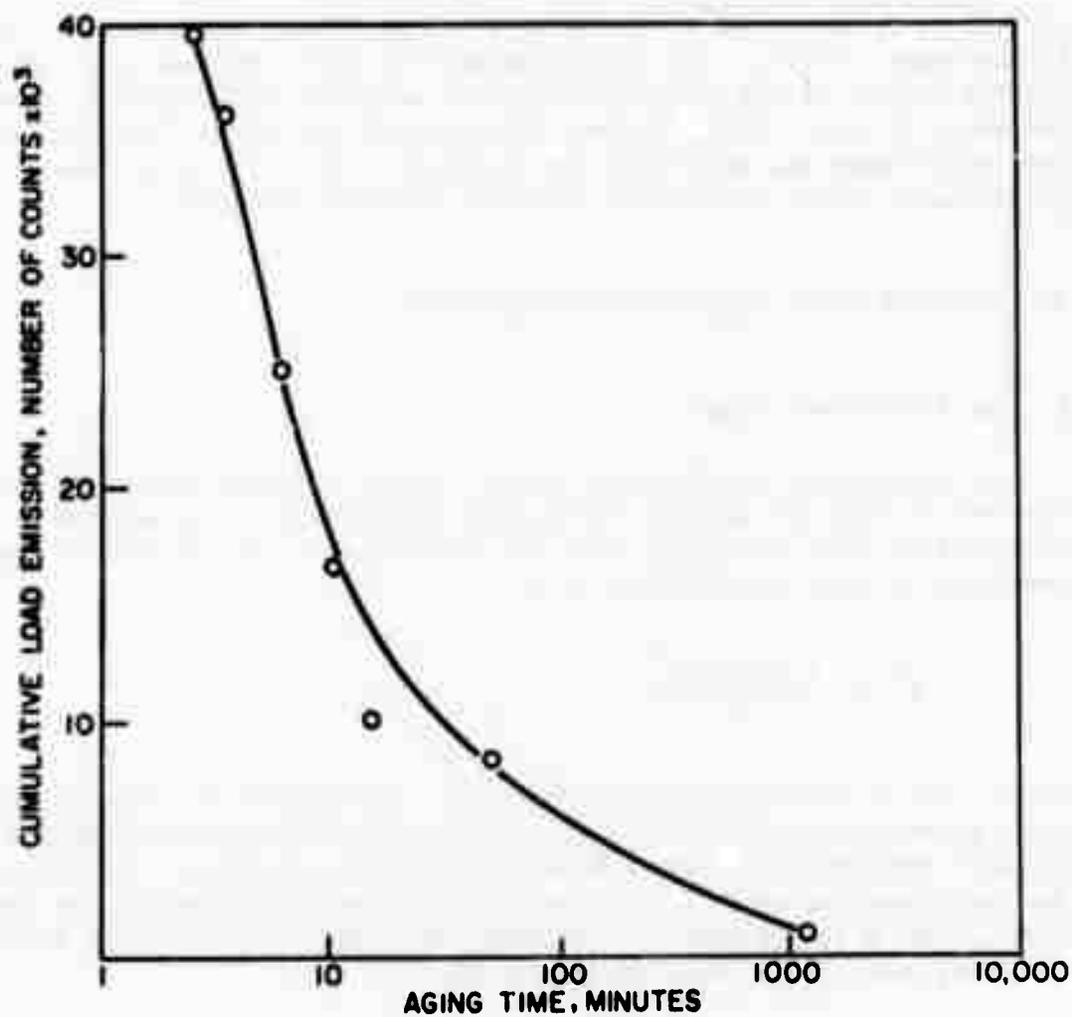
Figure 30. Dependence of the cumulative load emission from 2024 aluminum on aging time.

<u>Overaged 2024 aluminum</u>: Aging Al-4% Cu at 572°F (300°C) for 1 hr or Al-4.6% Cu at 482°F (250°C) for 48 hr gives an average $CuAl_2$ particle spacing in the range 1.0-2.5μ. The aging treatment in these experiments at 600°F (316°C) for 100 hr may therefore result in slightly higher spacing, namely in the range of 2-3μ. Figure 1 shows that part of this region falls within the detectable range and part below the threshold. The tests give a small but unquestionable number of acoustic emissions for this condition.

B. EFFECT OF GRAIN SIZE ON ACOUSTIC EMISSION

1. The Microstrain Range

It is possible to relate the width f of an activated Frank-Read dislocation source with the length L of the pile-up produced by it, and the number of dislocations which it emits. This has been shown[6] for the size of the specimens used in this investigation to be

$$L^3 = \frac{f \times 2 \times 10^4}{\pi} \tag{11}$$

where L and f are expressed in microns (μ). The activation shear stress σ_{act} for a given source width is known, and hence Eq. (11) gives the minimum slip distance required to produce a detectable acoustic emission. Table VI shows the calculated values of L, σ_{act}, and N for a range of values of the source width, where N is the number of dislocations produced in a pile-up before the resulting back stress shuts the source off.

TABLE VI

THE ACTIVATION SHEAR STRESS AND REQUIRED SLIP DISTANCE FOR
A RANGE OF DISLOCATION SOURCE WIDTHS

f (μ)	σ_{act} (kg/mm^2)	L (μ)	N
0.1	8.6	14	170
1.0	.86	30	37
10	.086	65	8
100	.0086	140	2

From dislocation etch pit studies a reasonable estimate of typical source widths in an annealed specimen is between 1μ and 10μ for all grain sizes. This estimate is based on the assumption that the average dislocation spacing

corresponds to the distance between pinning points on a dislocation line. Table VI shows that the shear stress required to activate such sources would vary from $1.0^{kg}/mm^2$ for f = 1 to $0.1^{kg}/mm^2$ for f = 10. For grain sizes larger than about 130μ, any such source which sweeps across an entire grain should be detectable.

The first acoustic emission activity, consisting of a few counts, is observed to be at about a $0.1^{kg}/mm^2$ (roughly 150 psi) tensile stress. There appears to be no systematic variation in the number of counts vs. grain size until a tensile stress of about $0.4^{kg}/mm^2$ (600 psi) is reached.

The small number of counts detected at a 0.1 V trigger level at a tensile stress below $0.4^{kg}/mm^2$ suggests that the typical microstrain events that occur in the microstrain region are not characterized by the activation of Frank-Read type sources. Some sources may have been activated, as counts were registered, but the bulk of the microstrain was probably the result of the relatively stable movement of mobile or loosely pinned dislocation segments. Such events would most likely not involve a large enough number of dislocations moving far enough simultaneously to produce a detectable emission.

The acoustic emission observations and the stress-strain observations suggest that during microstrain in 99.99% Al the glide distance is not defined by the grain size, at least for grain sizes larger than 100μ. A more likely explanation is that interactions between moving dislocations and forest dislocations provide the most important strengthening mechanism.

2. Effect of Grain Size on the Acoustic Emission
    Behavior in the Macrostrain Range

At tensile stresses of 0.4 to $0.5^{kg}/mm^2$ (600 to 750 psi), specimens with grain sizes larger than 200μ appear to have entered the macrostrain range. Macrostrain is characterized by a nearly flat appearance of the stress-strain curve, with the slope varying slightly with grain size. Acoustic emission data show a rather sudden increase in the rate of emission even before the macrostrain region is reached, at a tensile stress of about 450 psi for all grain sizes larger than 200μ. Once this high-rate-of-emission region is reached, the cumulative load emission ΣLE is approximately proportional to the applied stress. This implies that the rate of emission is approximately proportional to the plastic elongation, at least up to elongations of about 2%. Figure 15 shows the strong effect that the grain size has on this proportionality factor in the macrostrain region. These observations provide some clues as to how deformation—at least the deformation detected by the acoustic emission transducer—proceeds during macrostrain.

There are two phenomena that might give rise to the emissions detected during macrostrain. One is the widespread unpinning and coordinated movement of dislocations, and the other is the activation of dislocation sources.

53

Consider first the unpinning and coordinated movement of dislocations. If this is the controlling source of emissions it must explain both the uniform rate of emission with strain, and the observed effect grain size has on the cumulative load emission ΣLE behavior. Suppose that dislocations, upon being unpinned, are able to move across an entire grain and are stopped by grain boundaries. Such unpinning events may be envisioned to occur as an "avalanche" of dislocations spreading across a grain. The magnitude of such events should be roughly proportional to (grain size)^3, the number of dislocations involved being proportional to the grain size, and the slip area being proportional to (grain size)^2. This would predict that the total number of events activated at a particular value of plastic strain be proportional to (grain size)$^{-3}$. Plots of ΣLE versus grain size on the descending side of the peak, using some value of plastic strain rather than an applied stress level as the constant parameter show that ΣLE is roughly proportional to (grain size)$^{-2}$. This alone does not necessarily disqualify the model of unpinned dislocations forming avalanches that are stopped by grain boundaries, but the following considerations cast doubt on its validity.

The initial dislocation etch pit density of all recrystallized specimens was roughly 10^6 per cm^2. Using the relation

$$\frac{\text{Length of line}}{\text{Unit volume}} = 2 \times \frac{\text{Number of intersections}}{\text{Unit area}}$$

gives 2×10^6 cm/cm^3 as the length of dislocation line per unit volume in a specimen. Assuming that all of the initial dislocations are mobilized and move, on the average, a distance of 1/2 the grain size, the equation

$$\gamma = \frac{v \, M \, b \, \frac{D}{2}}{v}$$

expresses the maximum shear strain possible from the unpinning, and subsequent movement of initial dislocations alone. The volume of the specimen is v; M is the length of dislocation line per unit volume. The maximum elongation possible by this mechanism is about 0.15%. Hence, if unpinning is the major cause of the emissions detected, it requires that a continuous generation of dislocations occur concurrently. The assumption that the activation of dislocation sources is not the major cause of emissions further requires that the freshly generated dislocations undergo successive pinning-unpinning processes, and some possible secondary dislocation motion associated with them that give rise to the emissions.

So far, the unpinning model can adequately explain the observed uniform rate of emission with strain, but it is necessary to acknowledge the possibility of dislocation generation in order to account for the amount of strain over which uniform emission occurs. Further, it is necessary to justify the assumption that the activation of these sources is not the major cause of the detected

emissions. Intragranular obstacles provide opportunities for successive pinning and unpinning of the dislocations generated by the sources, and these unpinning actions cause most of the emission. The requirement that such intragranular obstacles be dominant implies that the grain boundaries must be masked as sources of emission behavior of a specimen. This is certainly not the case.

From these arguments it may be concluded that the major cause of the detected emissions, at least for a certain range of grain sizes, is not the unpinning of dislocations. This suggests that the activation of dislocation sources be considered as a mechanism leading to the generation of acoustic emissions.

Without going into a detailed discussion, source activation may be used as a model to explain the observed uniform rate of emission with increased applied stress. Each increment of applied stress activates a uniform additional number of dislocation sources. As an incidental point, this may imply that the distribution of sources is inversely proportional to the source width, i.e.,

$$\Delta LE \propto \Delta\sigma \Rightarrow \Delta N \propto \frac{1}{f}$$

where ΔN is the number of additional sources activated by the stress increment $\Delta\sigma$, and f is the average width of those sources activated as the stress increases from σ to $\sigma + \Delta\sigma$. Such a statement is complicated, however, by the possibility that new sources are created as strain proceeds.

The final question to be answered is "can the source activation model explain the observed variation in the rate of emission with grain size?" Assume first that there exists a grain size independent distribution of dislocation sources in a specimen. At a given level of applied stress, all sources down to a certain width should have been activated. It can be deduced from Table VI that the grain size is not likely to control the detectability of sources which are smaller than 10μ. Hence, such a model cannot easily explain the observed ΣLE vs. grain size variation.

Attempting to develop a satisfactory model involving the activation of dislocation sources, we focused on the grain boundaries themselves. We studied the changes in the appearance of slip lines in the microstructure of the 99.99% Al as the applied stress was increased from 300 psi to 900 psi in increments of 150 psi. The results of this effort indicate that slip in one grain activates slip on secondary systems in adjacent grains. These observations, combined with the observation that the grain size effect on the ΣLE versus grain size curve began to emerge at tensile stresses of about 600 psi motivated the proposal that the major cause of the emissions detected is the activation of dislocation sources near the grain boundaries when slip is propagated from one grain to its neighbor. This is essentially the intergranular slip model proposed by Cottrell,[16] and it will now be applied to the acoustic emission observations as a possible explanation of the ΣLE versus grain size variation.

C. THEORY OF THE SHAPE OF THE ΣLE VERSUS GRAIN SIZE CURVE

Intergranular slip occurs when plastic strain is propagated, by some mechanism, through a grain boundary. Typically, intergranular slip does not begin simultaneously throughout the entire specimen, but starts at a few localized regions and becomes more and more predominant as deformation proceeds.

Consider a typical grain boundary in a recrystallized specimen. Cottrell envisions the propagation of slip across a grain boundary to occur when the resolved shear stress at the head of a dislocation pile-up held up by the grain boundary reaches a critical value σ_o. A suggested mechanism was the activation of a Frank-Read source in the adjacent grain, near the grain boundary. If there are N dislocations in the pile-up, an applied shear stress σ exerts a stress $N\sigma$ on the grain boundary. The number of edge dislocations in a double pile-up is given by[17]

$$N = \frac{2(1-\nu)\sigma L}{Gb} \tag{12}$$

where L, in this case, is the distance from the source to the leading dislocation of the pile-up. If L is assumed to be equal to one half the average grain diameter D, the stress applied by the pile-up on the grain boundary may be taken as

$$N\sigma = \frac{2D\sigma^2(1-\nu)}{2Gb} \tag{13}$$

The validity of taking L as $D/2$ is questionable, particularly since the length of the dislocation pile-ups which were observed at a 0.8kg/mm^2 tensile stress was not seen to be controlled by the grain size. From a stress concentration standpoint, the effective length of a dislocation pile-up may have an upper limit determined by the surrounding dislocation network density.[18] The local stress induced by the pile-up may activate secondary sources in the network. These secondary sources may interact with the pile-up dislocations, effectively dividing a large pile-up into a series of shorter ones. Also Eq. (13) takes no account of the effect of blunting which, based on etch pit studies and the relative ease of cross slip in aluminum, probably occurs.

The typical acoustic emission data of Figure 10 indicated that up to a 200µ grain size, the applied stress needed to initiate the high-rate-of-emission decreases as grain size increases. For grain sizes larger than 200µ, little consistent effect upon the stress level at which high-rate-of-emission begins was observed. Data slip line studies showed that the initiation stress level corresponds fairly well with the stress level at which slip seems to begin to propagate across grain boundaries. Hence, it may be proposed that up to about 200µ, the grain size serves as an upper limit to the effective pile-up length, and that for greater than 200µ grain size the length of a typical pile-up is not controlled by the grain size.

If the length of a pile-up is L, and x is the distance ahead of the pile-up on its glide plane, the local shear stress at x (for x > 1) is approximately given by[18]

$$\sigma_x \simeq \sigma\left[1 + \frac{L}{2x}\right] \tag{14}$$

where σ_x is the local shear stress and σ is the applied shear stress. The significance of the above equation is that the stress concentration due to the presence of a pile-up is long range in nature. Hence, well into the grain adjacent to the one in which the pile up exists, the local shear stress is considerably higher than the applied shear stress. This factor should aid in the movement of dislocations across the adjacent grain at high velocities.

When the stress field due to the pile-up succeeds in triggering a dislocation source in the adjacent grain, the local stresses on the source are quickly relaxed to a level just below that necessary to operate the source. This quick relaxation of stress is caused by the nearness of the source to the grain boundary. A small increment in applied stress is necessary to cause a further increment of slip across the grain boundary. In effect, a large angle grain boundary is step-wise unstable as a slip obstacle. Figure 31 shows a possible sequence of events leading to a grain boundary "breakthrough." The proximity of the source S_2 to the grain boundary limits the number of dislocations it may emit in an unstable step to just a few, maybe from one to ten.

Suppose that there is a grain size independent density of grain boundary sources, such as S_2, per unit grain boundary surface area. Assume also that the width of these sources is grain size independent. Then, at a given applied stress, the number of these sources in a fixed volume which had been activated by local stress concentrations should be proportional to the total grain boundary surface area, which in turn is proportional to $D^2/D^3 = D^{-1}$, where D is the average grain diameter. This, of course, is assuming that the density of grain boundary sources, and not the density of dislocation pile-ups which reach the grain boundaries, is the parameter controlling the number of grain boundary sources that are activated.

If the grain boundary model can now adequately explain the observed acoustic emission behavior, in particular the ΣLE vs. grain size variation, it would be reasonable to state that it is the major cause of the acoustic emissions detected in polycrystalline Al specimens. It has been shown that the number of grain boundary sources activated should be proportional to D^{-1}. If N is the number of dislocations that take part in a slip event which produces acoustic
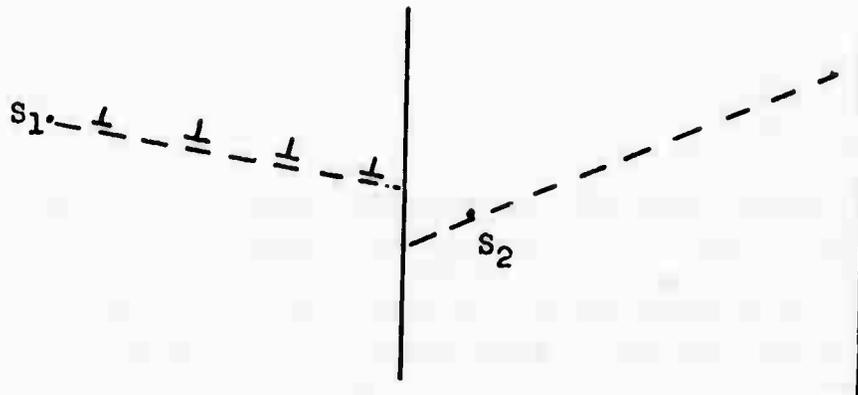
Applied stress activates source S_1, which produces a dislocation pile-up held up by the grain boundary.
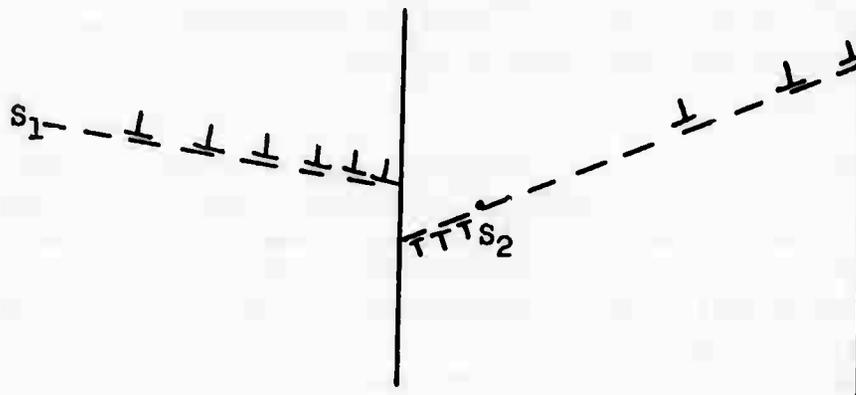
As the pile-up grows under increased stress, it activates the source S_2 in the adjacent grain.

Figure 31.   Grain boundary source mechanism.

emission and "a" is the minimum slip area necessary to produce an acoustic emission, and if N equal to 10 is taken as an upper limit to the number of dislocations produced in a single burst by one of the grain boundary sources, the minimum slip area that can yield a detectable emission from such a source is $10,000\mu^2$, and the corresponding grain diameter is about 320μ. Thus, a plot of the likelihood of detecting the activation of a grain boundary source, when the trigger level setting is 0.1 V, should be very small for grain sizes smaller than 100μ, increase continuously as the grain size increased from 100μ to 320μ, and undergo no further increase as the grain size increases beyond about 320μ. Between 100μ and 320μ, the rate at which the likelihood of detection increases with grain size is difficult to specify, being complicated by three factors:

1. There is certainly scatter in the grain size within a given specimen;

2. The actual slip area depends on the way in which the slip plane cuts across the grain; and

3. Dislocation obstacles such as Lomer-Cottrell barriers, impurities, and forest dislocations would result in a variation in the actual slip area swept out in a single step, with (grain diameter)^2 as an upper limit.

A plot of the total number of grain boundary source events detected by the transducer should be a plot of the product of the number of grain boundary sources activated (proportional to 1/D) times the likelihood of detecting a source. Figure 32 shows this function graphically. Notice that a peak is produced at a 320μ grain size.

At stresses on the order of $0.8^{kg}/mm^2$ to $1^{kg}/mm^2$, some intragranular dislocation sources should be detectable, in addition to the grain boundary a associated sources. Additional detectable events were seen, see Table VI. For grain sizes larger than 130μ, the cumulative activity produced by intragranular sources should not vary much with grain size even if the grain size does control the slip distance at stresses on the order of $1^{kg}/mm^2$. Hence, a constant level of activity may be added to the dashed curve of Figure 32(a) to give the total number of events one would expect to detect during a 0.1 V trigger level test. This total number is represented by the solid curve of Figure 32(a).

The behavior shown in Figure 16 is fairly well described by the solid curve of Figure 32(a). The theory developed accurately predicts the position of the peak, but does not predict the constant level of ΣLE for increasing grain size beyond about 1000μ.

In Figure 19 the peak in the ΣLE vs. grain size curve was observed to be less prominent for the case of the 0.2 V trigger level test than for the 0.1 V trigger level tests. Also, the peak occurred at a grain size of 400μ to 500μ in the 0.2 V trigger level tests.
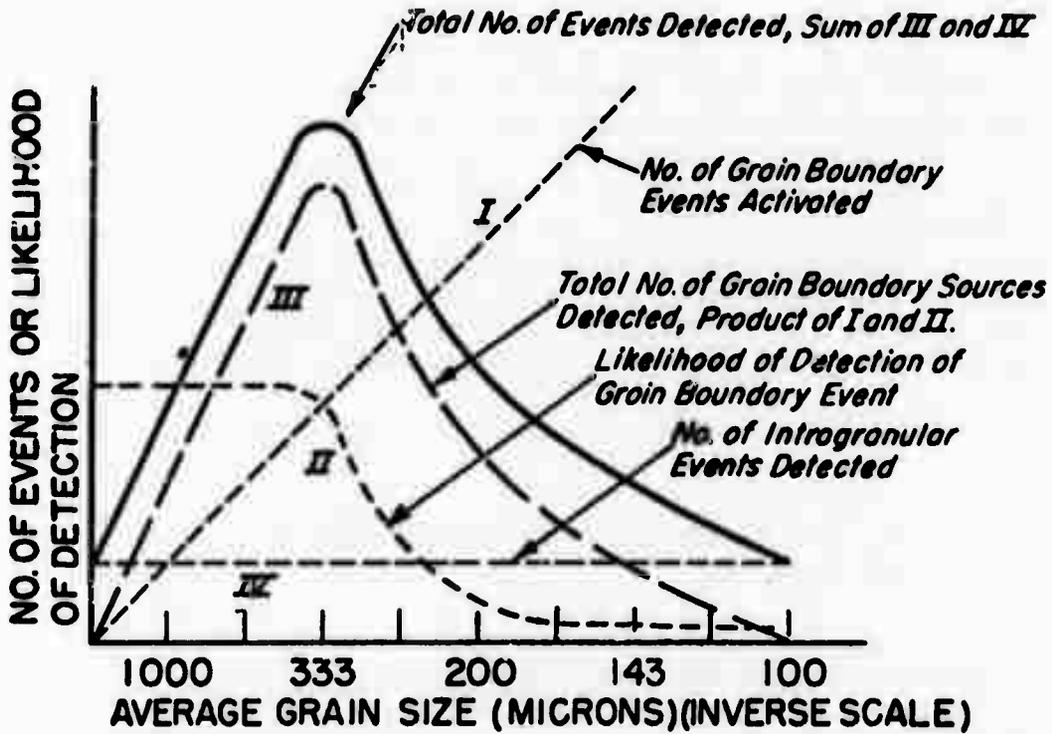
Figure 32(a). Graphical representation of acoustic emission behavior model based on the activation of grain boundary sources. 0.1 V trigger level.
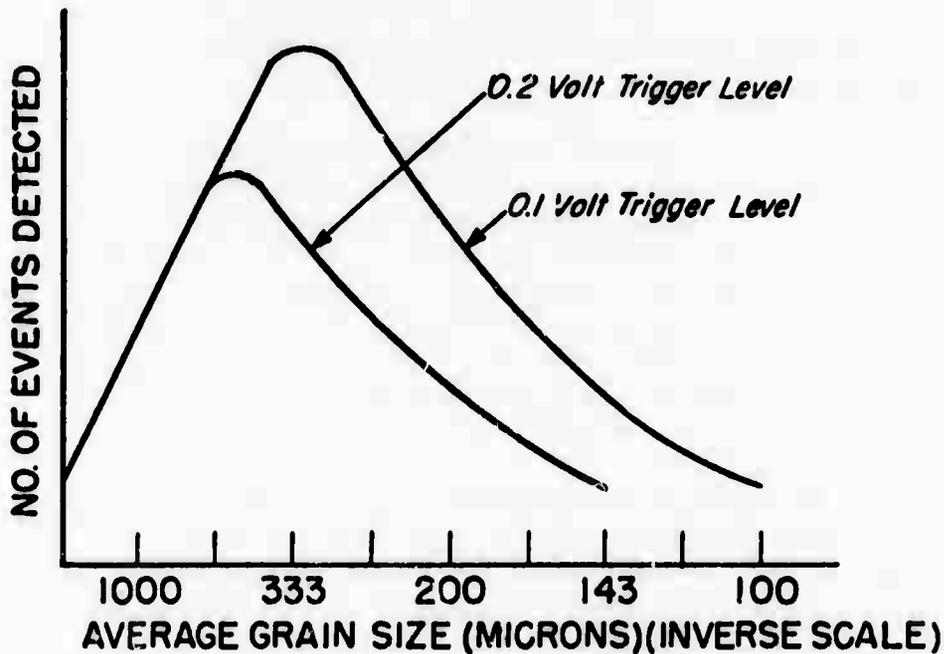
Figure 32(b). The calculated effect of changing the trigger level setting.

The shift in the position of the peak for the 0.2 V trigger level tests is to be expected for the following reason. In doubling the trigger level, by changing it from 0.1 V to 0.2 V, the minimum detectable surface displacement "a" is doubled. If the relationship between the number of moving dislocations and the minimum detectable area, namely,

$$N_a = 10^{-7} \, (\text{meter})^2 \tag{15}$$

is assumed to be valid[19] then the smallest slip area that can yield a detectable emission from a grain boundary source (set N equal to 10) is $20,000\mu^2$, corresponding to a grain size of 141μ. Similarly, the saturation condition (set N equal to one) occurs at a grain size of 451μ, which is larger by a factor of $\sqrt{2}$ than the saturation condition for the case of a 0.1 V trigger level. Thus, it is to be expected that doubling the trigger level should translate the position of the peak by a factor of $\sqrt{2}$ to a larger grain size. This accurately describes the observed effect of raising the trigger level from 0.1 V to 0.2 V.

In view of the approximate nature of the analysis, the observed positions of the peaks in the 0.1 V and 0.2 V trigger level curves appear to be in good agreement with the theory developed.

D. ACOUSTIC EMISSIONS FROM 99.99% Al SPECIMENS THAT HAVE BEEN SUBJECTED TO A RECOVERY HEAT TREATMENT

Because of the nature of subgrain walls and the comparatively small slip area available within a subgrain, the grain boundary source mechanism that was proposed to account for the behavior of the recrystallized specimens is not applicable to the case of the recovered specimens in which subgrains are present. Any microstrain event which is constrained to within a single subgrain will be unlikely to result in a detectable acoustic emission. This may be seen by considering Table VI and recalling that the largest subgrains under consideration are only about 20μ long.

It is probable that the initial emissions produced in the recovered specimens result from the movement of loosely pinned subboundary dislocations. These sources of emission are exhausted, and further emission probably comes from subboundary breakthrough events. Only under special circumstances can the breakthrough events give rise to emissions, thus the small number of counts produced as the tensile stress increases beyond the 1 kg/mm^2 range. Deformation must proceed mostly by the process of dislocation movements and source activation that do not involve more than one or two subgrains.

E. ACOUSTIC EMISSION FROM METALS DURING THE REMOVAL OF STRESS

1. Conditions to Produce Reverse Plastic Strain

The following discussion on the conditions necessary to initiate reverse plastic deformation on unloading is based upon works by Cottrell,[21] Nabarro,[22] and Kulhmann.[23]

To initiate motion of an already existing dislocation in a polycrystal, a stress σ_i acting on the dislocation has to be overcome. σ_i is the maximum value of the fluctuating internal stress field, which is the result of the resistance to the motion of the dislocations caused by various irregularities such as foreign atoms, precipitated particles and other dislocations. The dislocations can be assumed to be moving through a potential field of energy hills and valleys of constant maximum slope σ_i. When the applied stress σ_1 exceeds the internal stress field σ_i, slip takes place. Dislocations tend to pile up against either obstructions that already exist such as a grain boundary, or those that are created due to dislocations in different planes intersecting, such as Lomer-Cottrell locks. Let σ_d be the back stress due to dislocation pile-ups at the obstacles. The dislocations have moved forward until

$$\sigma_1 = \sigma_i + \sigma_d \tag{16}$$

Consider what happens when the applied stress σ_1 is reduced to $\sigma_1-\Delta\sigma$. If $\Delta\sigma$ is less than $2\sigma_i$ the dislocations move no farther than across one valley. The internal stress decreases from σ_i to $\sigma_i-\Delta\sigma$ to restore equilibrium. The minimum value to which the internal stress can reduce to is $-\sigma_i$

$$\sigma_1-\Delta\sigma = \sigma_d-\sigma_i \tag{17}$$

From Eqs. (17) and (18) it is clear that as long as the dislocation motion is limited to the distance across one valley, the resulting plastic strain is small.

When the reduction in the applied stress $\Delta\sigma$ is greater than twice the value of the internal stress field, i.e., $\Delta\sigma > 2\sigma_i$ equilibrium can only be restored by a reduction in the value of the back stress σ_d. This means the dislocation had to move farther than across one valley. The resulting plastic flow is easily perceptible. Thus the only condition to be satisfied to cause reverse flow is $\Delta\sigma > 2\sigma_i$.

It can easily be seen that if $\sigma_1 >> 2\sigma_i$ and the applied stress is then reduced to zero, reverse plastic flow can take place during unloading as shown in Figure 33.
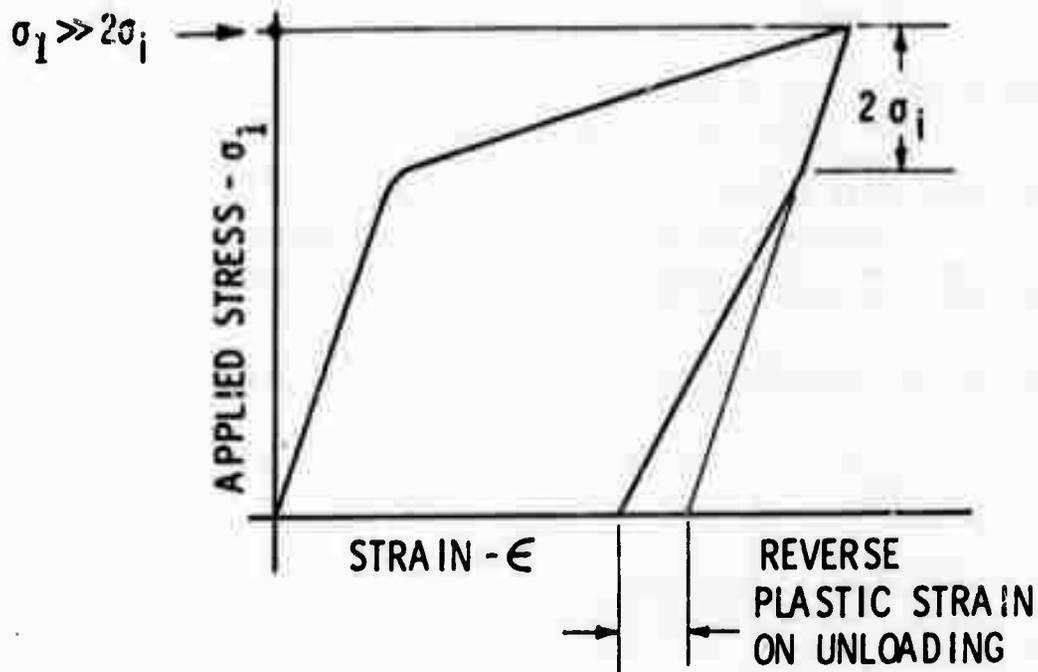
Figure 33. Reverse plastic flow on unloading.

The principal forces resisting the motion of a dislocation in a metal lattice are the following:

1. The resistance offered to dislocation motion between two successive equilibrium positions, i.e., the force required to overcome the potential separating the two equilibrium positions, a lattice spacing apart. This is the Peierls-Nabarro force.

2. The resistance due to point defects in the lattice, precipitate particles and other dislocations. The spacing of these defect sites is much larger than one atomic spacing.

3. The resistance offered to dislocation motion by grain boundaries and subgrain boundaries.

A resistance can act as a friction stress or a back stress during the process of unloading, depending upon the extent of dislocation motion. If the motion is limited to two successive equilibrium positions of dislocations, a lattice spacing apart the interaction stress will be a back stress and the only friction stress will be the Peierls-Nabarro stress. If we consider the long range motion of dislocations shearing through several bariers such as precipitate particles, the internal stress due to particles will act more like a friction stress. It can be assumed that at small ranges of stress, slip is

63

limited to within the grains and the resistance that a grain boundary offers becomes more of a back stress. Deak[20] classifies this as a "long-range" back stress whereas back stress due to closely spaced point defects are termed "short-range" internal stresses.

During the process of deformation, it is likely that some dislocations are stopped by closely spaced point defects. Many more may get piled up against strong barriers such as grain boundaries. While unloading, the short range back stresses relax first as they have to overcome only the Peierls-Nabarro force. It is useful to calculate the order of strain that results when the short range back stresses relax. This simply means that the dislocation motion is limited to motion over a distance lying in between the defects.

The spacing of solute atoms in a solid solution is given by

$$\Lambda = b/c^3$$

where Λ = spacing of solute atoms,
c = concentration of solute,
b = Burgers vector.

We can calculate the strain when the dislocation moves in between two solute atoms. Since the strain that results due to motion of a dislocation between two solute atoms spaced a few atomic distances apart is smaller than that due to motion of the dislocation incoherent precipitate particles in an overaged alloy, the following calculations are done for an overaged alloy. The results will indicate that unless several dislocations move at one time or one dislocation moves through several particles, even inter-particle motion cannot be detected.

Let us assume a 2μ spacing between particles in an overaged alloy. Let the dislocation move through an average distance of 1μ, under the application of a stress. The resulting shear strain

$$\gamma = N'.b.A_s$$

where N' = number of mobile dislocations, per unit volume,
b = Burgers vector, and
A_s = area swept by a unit length of dislocation.

For one single dislocation, with an average displacement of 1μ the shear strain is $\gamma = 1 (2.83 \times 10^{-8}) (1 \times 10^{-4}) = 2.83 \times 10^{-12}$. In an undeformed specimen of annealed aluminum, the dislocation density is of the order of 10^5 to $10^6/cm^2$. If we assume a dislocation density of $10^6/cm^2$ between two precipitate particles spaced two microns apart, the number of dislocation lines is less than one. It can thus be seen that the number of available mobile dislocations is small and

so is the strain.

The minimum strain detection capability of the acoustic emission instrumentation used in this investigation is 0.85×10^{-10} in./in. Hence, intraparticle motion of the dislocation is unlikely to be detected unless motion between several particles takes place at one time. Thus, the major contribution must be due to the relaxation of long range back stresses when the dislocations pile up against the grain boundaries and move through or around several particles.

2. Role of Cross-Slip in Reverse Plastic Deformation

The above argument for reverse plastic deformation implies a basic assumption, i.e., that there are enough mobile dislocations in the slip plane to give the deformation on unloading.

At the start of the third stage or near the end of the second stage of deformation, Seeger[24] observed coarse slip in copper and aluminum replicas. At this stage, the slip lines cluster together to form bands which are comparatively short and connected to other bands by slip. The connecting slip is called cross-slip. This is a characteristic feature in the deformation of aluminum. Obstructions to dislocation motion such as Lomer-Cottrell locks in the primary slip planes cause screw dislocations or screw components of edge dislocation loops to cross-slip to alternate planes which have a common slip direction. The ease of cross-slip depends on the stacking fault energy of the material. To cross-slip, the two partial dislocations have to first come together to form one dislocation. In the case of a metal with low stacking fault energy, the partials are widely separated and the energy needed to force the partials together is higher. Hence, cross-slip does not take place easily. On the contrary, aluminum, with a stacking fault energy of about 200 ergs/cm^2[25] exhibits cross-slip even under low stresses at room temperature.

Seeger[26] obtains the following expression for the shear stress necessary to combine two partial dislocations at the head of a pile-up of dislocations and thus initiate cross-slip.

$$\tau = \frac{1}{n} \left[\frac{\sqrt{2}\, G}{4\, \pi} - \frac{2\gamma_s}{b} \right] \tag{18}$$

where τ = shear stress necessary to initiate cross-slip,
n = number of dislocations in the pile-up,
G = shear modulus,
γ_s = stacking fault energy, and
b = Burgers vector.

The number of dislocations in the pile up is given by

$$n = \frac{\pi \tau L}{Gb}$$

where L is the maximum glide distance. L is approximately equal to half the grain diameter, D, in a high purity material. Precipitate particles, subgrain boundaries, etc. reduce the slip distance. Equation (19) can therefore be written as

$$\tau = \frac{Gb}{\pi \tau L} \left[\frac{\sqrt{2}G}{4\pi} - \frac{2\gamma_s}{b} \right]$$

$$\tau^2 = \frac{Gb}{\pi L} \left[\frac{\sqrt{2}G}{4\pi} - \frac{2\gamma_s}{b} \right]$$

or

$$\tau = \left[\frac{Gb}{\pi L} \left(\frac{\sqrt{2}G}{4\pi} - \frac{2\gamma_s}{b} \right) \right]^{1/2} = \left[\frac{\sqrt{2}G^2 b}{4\pi^2 L} - \frac{2\gamma_s G}{\pi L} \right]^{1/2}$$

Certain results are apparent on interpreting the above equation. They are as follows:

1. Larger grain size decreases the shear stress necessary to initiate cross-slip. For the same plastic strain, larger grains will contain a longer pile-up and will undergo cross-slip at a lower stress.

2. Higher stacking fault energy allows cross-slip at lower stresses.

3. Any condition that decreases the glide distance increases the stress necessary to initiate cross-slip.

From transmission electron microscope observations, Feltner and Laird[27] defined slip character as planar or wavy depending on the degree to which the dislocations are confined to individual slip planes. Aluminum, aluminum-magnesium alloys, copper, pure dilute iron-carbon alloys, etc., show wavy slip mode. Copper-aluminum alloys and brass show planar slip mode. Feltner and Laird[27] observed a dislocation structure that is confined to one plane in a copper-7.5% aluminum alloy subjected to cyclic stresses. No dislocation dipoles were observed. Also 70-30 brass, cyclically strained at small amplitude, showed straight dislocations forming many multipoles. For very small plastic strains, few complex dislocation interactions occur. On unloading, the short range internal stresses move the dislocations over their own debris. It is likely that more dipoles are formed by the cross-slip. Therefore, the magnitude of friction stress might increase as the dipole density increases during loading and unloading.

Materials that exhibit planar slip mode show considerable reverse plastic deformation on unloading. Feltner and Laird[28] observed a deformation as high as 15% to 20% of the prestrain in copper-7.5% aluminum alloy, annealed, whereas high purity annealed copper did not show any deformation on unloading. The Bauschinger tests conducted on a copper-7.5% aluminum alloy during this investigation confirm this. It can be concluded that the reversal of dislocation motion is much easier in a planar mode material for the following reasons:

1. Slip is confined to primary planes because of reduced cross-slip activity.

2. The dipole obstacle density is very low.

3. The reverse dislocation motion, aided by long range back stresses, takes place easily. The opposite is the case with wavy slip mode materials.

The above discussion on reverse plastic deformation can be summarized as follows:

1. Reverse plastic deformation on unloading is possible if the applied stress exceeds twice the value of the internal stress, ($\sigma_1 >> 2\sigma_i$ to be observable) and if the decrease in the applied stress $\Delta\sigma$ is greater than twice the value of the internal stress σ_i, i.e., $\Delta\sigma > 2\sigma_i$.

2. Significant reverse deformation is observed in planar slip mode materials because there is less cross-slip and dislocations are thus generally confined to primary slip planes.

3. There is a certain minimum strain pulse that the measuring system is capable of picking up. Hence, most slip in the secondary systems will not be picked up by the detection system.

The above explanation is among the possible mechanisms that can explain the observed unload emission behavior. Increased resistance to dislocation motion due to interaction with forest dislocations might prevent the dislocations from moving back.

The unload emission behavior of various materials is discussed in the light of the above conclusions.

F. UNLOAD EMISSION IN 99.99% ALUMINUM, AND 6061 AND 2024 ALUMINUM ALLOY

From Seeger's[26] equation, the applied stress to initiate cross-slip in a polycrystalline 99.99% aluminum sample, annealed at 970°F for 3 hr is calculated as being about 800 psi. The average grain size of the sample was about 1500μ. Among all the materials tested, 99.99% aluminum gave the least unload emission

67

as can be seen in Figure 23 which compares unload emission behavior of various materials for the same plastic strain. It is more meaningful to compare emission at the same strain as the dislocation interaction can be assumed to be similar for this condition. The low unload emission in high purity aluminum is explained as follows. If other factors do not interfere, slip distances are larger in large grain specimens and there are more strain pulses whose amplitude lies above the detection capability of the measuring system. This is verified by the large amount of acoustic emission obtained during loading in 99.99% aluminum. The ease of cross-slip at lower stresses, however, reduces the availability of dislocations in primary planes which might possibly move back and give rise to reverse deformation. Though friction stresses are low, cross-slip seems to be the predominant factor in controlling the amount of reverse deformation. Figure 11 shows a drop in unload emission at a stress of about 2200 psi (at a strain approximately equal to 0.2%). This is due to increased cross-slip activity as well as increasing obstructions to dislocations and other forms of frictional stresses.

The effect of grain size on the unload emission of 99.99% aluminum is shown in Figure 13. In large-grain polycrystalline material, the deformation might take place on a single slip system but as the stress is increased, several slip systems become operative. In fine-grained specimens, deformation is essentially by multiple slip. Whereas a large grain specimen shows a decrease in unload emission at a lower stress of about 3100 psi, the unload emission curve for a fine-grain specimen shows no drop in emission activity within the stress levels used in this investigation, as can be seen in Figure 13, even though a much smaller number of emission counts is involved. Slip takes place in smaller strain increments in fine-grain samples.

For the 125μ grain size sample, the applied stress to initiate cross-slip is about 2360 psi. It can thus be assumed that extensive cross-slip activity exists at a stress of about 3000 psi and hence, the appearance of a drop in the unload emission beyond this stress level. For the 15μ grain size sample, the applied stress to initiate cross-slip is about 6750 psi. It is seen from Figure 13 that the unload emission, though small in fine grained samples does not show a tendency to decrease at stresses as high as 5000 psi.

Another factor might also contribute to the reduction in unload emission counts in larger grain material. Segal and Partridge[35] have reported changes in the dislocation density at various stages in uniaxial deformation of 99.99% aluminum. The average density of the dislocations in an annealed specimen is $5 \times 10^6/cm^2$. In specimens stressed up to 1350 psi, most of the regions appear similar to the annealed material. At 2700 psi, there are more regions where the dislocation density is as high as $2 \times 10^8/cm^2$, though there are large regions which still contain no dislocations. However, at about 4000 psi there is a tendency for dislocations to form groups. The dislocations are also shorter and more numerous. This means that as the deformation proceeds, slip distances become smaller and smaller. It becomes increasingly difficult for the dislocation to move back when the applied stress is relaxed due to more dislocation interaction.

68

Figure 23 shows a comparison of the unload emission counts of 99.99% aluminum, aluminum-copper 2024 and aluminum-magnesium 6061 alloys. The aluminum alloys show a slightly larger value of unload emission than the 99.99% aluminum. The grain size of these alloys is much smaller than that of 99.99% aluminum. Turnbull[25] gives a value of 117 ergs/cm^2 for the stacking fault energy of an aluminum-1% magnesium alloy. Pure aluminum has a stacking fault energy of about 200 ergs/cm^2.[25] This, together with increased drag resistance, makes cross-slip more difficult in these alloys. Figure 21 shows a drop in the unload emission at about 8750 psi for annealed 6061 aluminum alloy. A 2024 aluminum alloy will show cross-slip at much higher stress. Seeger's equation gives a value of 14028 psi as the applied stress to initiate cross-slip in 2024-T6 aluminum alloy specimen. Figure 22 shows that the unload emission drops at about 15000 psi in an annealed 2024 aluminum alloy.

The unobstructured slip distance will be largest in supersaturated solid solution and diminishes as the precipitation process commences. This will increase in the overaged condition. Thomas and Nutting[29] report mean slip distances of 3000 Å when the microstructure contains G-P zones, 400 Å when the microstructure contains θ" precipitate, and 700 Å when it contains the coherent θ' precipitate. When the structure consists of an incoherent precipitate θ, cross-slip and the slip lines are wavy. Thus the following conclusions can be stated.

1. In the case of solution treated alloys, the slip decreased are sufficiently large so the strain pulses are easily picked up by the detection system, whereas the strain pulses are too small for alloys that are aged to produce peak hardness.

2. The tendency for cross-slip is much lower in overaged alloys as is evident from the shape of the hardness vs. unload emission curves in the case of 6061 and 2024 aluminum alloys.

It is of interest to compare this result with the Bauschinger effect in 2024 aluminum alloys with different microstructures and with the results of Abel and Ham[14] on the effect of microstructure on the Bauschinger effect in 2024 aluminum alloy as shown in Table IV. Table IV indicates the possibility of a relationship between the unload emission and Bauschinger effect in this alloy. However, it must be borne in mind even when it is known that there is a deformation on unloading this does not necessarily mean that emission can be detected by the measuring system. The intensity of the strain pulses must be above the minimum strain detection capability of the system.

G. COPPER-7.9% ALUMINUM ALLOY

Copper-7.9% aluminum is a single phase alloy and the specimen used in this investigation had a grain size of about 50μ. The stacking fault energy is approximately 4 ergs/cm^2.[30] Among the fcc metals and alloys tested, this alloy showed the largest unload emission for the same amount of strain, as can be seen

in Figure 23. The stress to initiate cross-slip is quite high. Electron micro-
scope studies indicates slip to be planar and confined mostly to primary planes.
It would, therefore, be expected that under the absence of cross-slip, and with
less friction stress due to the absence of second phase particles, unload emis-
sion should be quite high. This is verified in Figure 23. The copper-7.9% alu-
minum alloy showed 3 to 5 times the unload emission that was obtained on a 2024
aluminum alloy of the same hardness, namely about 70 R_E.

H. THE KAISER EFFECT IN COPPER-7.9% ALUMINUM ALLOY

One of the interesting observations in the copper-7.9% aluminum alloy is the
absence of a complete Kaiser effect. An unstable Frank-Read source has been
proposed as the cause of load emission in aluminum and aluminum alloys. In the
case of repeated loading, sources of suitable length all operate during the first
loading, and in the second loading no other source operates until the previous
stress level is exceeded. This hypothesis, however, assumes that there is no
rearrangement of dislocations during unloading, a situation more likely to happen
in the materials that Agarwal tested, where the tendency for the dislocations to
move back is small. It is hypothesized here that the dislocations that move back
on unloading can move forward on reloading thus giving emission on second load-
ing. This emission on second loading cannot be expected to be high as in the
first loading.

The absence of a Kaiser effect in the fcc alloys can perhaps be explained
on the basis of a model proposed by Makin.[33] He postulates that locks are
formed during unloading and that these locks are broken on subsequent loading.
His evidence for this is the reappearance of a yield point phenomenon on a
second application of a load to a single crystal tensile specimen of 99.99%
copper. The yield drop is directly proportional to the decrease in stress dur-
ing unloading.

Since there are fewer slip systems to operate, the chances of Lomer-Cottrell
locks forming in copper-7.9% aluminum alloy is decreased though it cannot be
completely ruled out. Instead, it can be assumed that the dislocation in the
active slip planes can move back and forth and that the ease of their motion
depends on the nature of the friction stresses. While unloading, the disloca-
tions are acted upon by the back-stresses. They move a certain distance, and
then stop when they encounter an obstacle. The back stresses cannot be relieved
except by thermal means. The back-stress builds up until it is sufficient to
cause dislocations to shear through the barriers. This planar motion of disloca-
tions can take place back and forth depending on the direction of the effective
stress.

I. 99.95% MAGNESIUM

It has been hypothesized above that if slip is confined to primary planes
there is a greater likelihood of dislocations moving back and forth. If this

were true, hcp metals, with slip confined to basal planes, should show more pronounced effect. ,

99.95% magnesium samples were rolled to 1/8 in. thick and annealed. The amplitude of the emission bursts, load as well as unload, observed in this material were larger than in any other material tested during this investigation. The unload emission counts, as well as the emission on reloading, were found to be highest in magnesium of all materials tested. The Kaiser effect is not apparent in this alloy, probably because slip is confined to basal planes, especially at low stresses. The maximum applied stress did not exceed 5000 psi in the acoustic tests. Because the critical resolved shear stress for basal slip is 1/20 to 1/100 of that for pyramidal or prismatic slip, basal slip account for most of the deformation. Kelly and Hosford[34] obtained stress-stain curves for magnesium of comparable purity for single crystals, textured polycrystalline materials with randomly oriented grains. The orientation of the specimens used in this investigation is comparable to the orientation designated as ZR in their work. It is reported that basal slip is more favorable in a large percentage of the grains in this orientation. The twinning mode is not predominant, especially in the stress range employed in the acoustic tests. The strain due to twinning is estimated to be less than 10% of the strain to which the specimens were subjected.

J. 70-30 BRASS

Annealed 70-30 brass specimens show considerable unload emission as seen in Figure 23. The stacking fault energy of 70-30 brass is reported as 10 ergs/cm^2.[31] 70-30 brass exhibits mostly planar slip with a few dislocation dipoles. The large load emission and the absence of the Kaiser effect are consistent with the above hypothesis for unload emission response.

K. THE DEPENDENCE OF THE UNLOAD EMISSION ON THE
   MAGNITUDE OF THE BAUSCHINGER EFFECT

It is of interest to compare the dependence of the unload emission on the amount of strain for several annealed fcc materials. Figure 23 showed a plot of strain vs. unload emission. It can be seen from Figure 23 and Table V that as the stacking fault energy decreases in fcc metals, the unload emission increases for the same plastic strain. In Table V it can be seen that there is a correlation between the Bauschinger strain, stacking fault energy and unload emission counts can be noted. The copper-7.9% aluminum alloy of all the fcc material, shows the largest unload emission counts and the largest Bauschinger stain, whereas 99.99% aluminum exhibits the least Bauschinger strain and the lowest unload emission.

VI. CONCLUSIONS

The following conclusions may be drawn on the basis of the results of the investigations that are being reported here:

(1) A plausible source of acoustic emission is the activation and subsequent shutting off of sources of dislocations.

(2) In 99.99% aluminum and 99.9% copper, these sources are generally associated with grain boundaries and their activation marks the onset of macrostrain.

(3) Whether or not any acoustic emission resulting from the activation of dislocation sources will be detected depends on the slip region diameter, and the source length, as well as on the sensitivity of the detection system and the background noise level.

(4) The dominant source of acoustic emission from 99.99% aluminum in the microstrain range ($< 5 \times 10^{-4}$) is intragranular and not associated with grain boundaries. It is due to the early movement of loosely pinned dislocation segments, possibly from the subgrain walls.

(5) The onset of macro-yielding in 99.99% aluminum and 99.9% copper occurs with the help of dislocation pile-ups held up by grain boundaries. The length of these pile-ups is independent of grain size for grains that are larger than about 200μ in diameter.

(6) The acoustic emission during macrostrain result from the activation of dislocation sources near the grain boundaries.

(7) Acoustic emission occurs in some materials when the applied stress on these materials is removed.

(8) When the peak magnitude of the stress is increased, the unload emission increases, reaches a peak value, and then decreases in all the fcc materials tested in this investigation.

(9) There is a good correlation between the unload emission and the Bauschinger effect. Materials that exhibit large unload emission show a large Bauschinger effect.

(10) The unload emission depends on the grain size of the specimen. In a large grain-sized sample, there are more strain pulses of amplitude above the threshold level of the measuring system because of larger glide distances.

(11) Materials that exhibit large unload emission do not show a complete Kaiser effect, i.e., they do show some acoustic emission on repeated loading.

It is likely that as long as the dislocations are confined to move in primary slip planes they can move back and forth during unloading and repeated loading and produce acoustic emission. Planar glide materials such as ε copper-7.9% aluminum alloy behave in this manner.

(12) Experimental results support the following explanation for the acoustic emission behavior of materials during unloading. Unload emission is the result of reverse plastic deformation. However, dislocations must be available in the primary slip planes to allow reverse plastic deformation of sufficient magnitude to be detectable as acoustic emission. Cross-slip reduces the availability of the dislocations in the primary slip planes to move back. Since the tendency for cross slipping is greater in materials with high stacking fault energies, materials such as 99.99% aluminum give low acoustic emission during unloading. On the same basis, a planar glide material, such as a copper-7.9% aluminum bronze, and a 70-30 brass show considerable unload emission because they have a low stacking fault energy. For the same plastic strain, the emission from copper-7.9% aluminum alloy is five to six times that of 99.99% aluminum.

(13) The use of low level acoustic emission of non-crack origin to monitor creep and fatigue processes is difficult in high strength alloys because of the need to keep the unwanted background noise to a minimum level at all times for the duration of the tests.

(14) The "unload" emission can possibly be used as a means of measuring the maximum value of the residual stress in a test specimen, but the low level of the emission and the consequent experimental difficulties preclude its use as a practical test method.

(15) The use of thermally induced stresses offers a quiet method for producing acoustic emission. The difficulties in predicting the absolute value or the distribution of the stresses limits this technique to those situations where these factors are not important.

VII. RECOMMENDATIONS FOR FUTURE RESEARCH

On the basis of the work done in the program the following appear to be promising areas for further effort.

(1) Use of acoustic emission originating from plastic deformation to assist in predicting ductile crack behavior. Plastic deformation takes place in front of and simultaneously with the propagation of a ductile crack.

(2) Use modern data processing techniques to analyze the acoustic emission signals. Much more information exists in the acoustic emission than in now being utilized. Signal-to-noise ratios could be improved. Information about the type of crack, what is going on in the vicinity of the crack, and the characteristics of the propagation path of the acoustic energy could possibly be obtained by such efforts. An initial step would be to investigate the spectra of the emission.

(3) Develop ways for using acoustic emission to monitor or measure the strain-hardening characteristics of materials.

(4) Develop acoustic emission as technique for nondestructively determining or monitoring various microstructure parameters of metals, such as dislocation density, the amount and distribution of one phase dispersed in another, such as results from aging or tempering, or for determining the percent of cold work in a metal.

(5) Develop specialized facilities for fatigue and creep testing high strength alloys with the necessary minimum of electrical and mechanical background noise. If this were done, it should then be possible to obtain useful predictive information based on acoustic emission. This can be done by making improvements in the equipment and by the use of electronic gating techniques.

REFERENCES

1. Nuclear Safety Quarterly Report, Aug.-Oct. 1968, Battelle-Northwest, Richland, Wash., p. 3.16 (Dec. 1968).

2. Michaels, T. E., "Acoustic Emission of Zircaloy-2 During Tensile and Fatigue Loading," Battelle-Northwest, Richland, Wash., Report No. BNWL-727 (Aug. 1968).

3. Dunegan, H. L., D. O. Harris, and A. S. Tetelman, "Detection of Fatigue Crack Growth by Acoustic Emission Techniques," Seventh Symposium on Nondestructive Evaluation of Components and Materials in Aerospace, Weapons Systems, and Nuclear Applications, Southwest Research Institute, San Antonio, Texas, pp. 20-31 (1969).

4. Engle, R. B. and H. L. Dunegan, "Acoustic Emission: Stress Wave Detection as a Tool for Nondestructive Testing and Material Evaluation," International J. Nondestructive Testing, 1, p. 109 (1969).

5. Moore, J. F., S. Tsang, and G. Martin, "The Early Detection of Fatigue Damage," AFML-TR-71-185 (1971).

6. Agarwal, A. B. L., "An Investigation of the Behavior of Acoustic Emissions from Metals and a Proposed Mechanism for its Generation," Doctoral Thesis, The University of Michigan (1968).

7. Eashelby, J. D., F. C. Frank, and F.R.N. Nabarro: Phil. Mag., Vol. 42, p. 351 (1951).

8. Hirth, J. P. and J. Lothe: Theory of Dislocations, p. 683, McGraw-Hill Book Co., New York (1968).

9. Ibid., p. 700.

10. James, D. R., "An Investigation of the Relationship Between Acoustic Emission and Dislocation Kinetics in Crystalline Solids," Ph.D. Thesis, University of Denver (June 1970).

11. Bilello, J. C. and M. Metzger, "Microyielding in Polycrystalline Cu," Transactions AIME, 245, p. 2279 (1969).

12. Li, J.C.M., "Petch Relation and Grain Boundary Sources," Trans. AIME, 227, p. 239 (1963).

13. Westmacott, K. H., "Hardening in Quenched Al," Philosophical Magazine, Series 8, 14, p. 239 (1966).

REFERENCES (Continued)

14. Abel, A. and R. K. Ham, "The Cyclic Behavior of Crystals of Aluminum—4 wt % Copper-I, The Bauschinger Effect," Acta Met., Vol. 14, p. 1493 (Nov. 1966).

15. Greethan, G. and R.W.D. Honeycombe, "The Deformation of Single Crystals of Aluminum—4.5 Percent Copper Alloy," J. Inst. Metals, 89, p. 13 (1960-61).

16. Cottrell, A. H., Dislocation and Plastic Flow in Crystals, Oxford at the Clarendon Press, London, p. 116 (1953).

17. Hirth, J. P. and J. Lothe, Theory of Dislocations, McGraw-Hill Book Co., New York, p. 683 (1968).

18. Friedel, J., Dislocations, Addison Wesley Publishing Company, Inc., Oxford, p. 263 (1964).

19. Bill, R. C., "An Acoustic Emission Study of the Deformation Mechanisms of Polycrystalline Aluminum and Copper," Ph.D. Thesis, The University of Michigan, Ann Arbor, Michigan (1970).

20. Deak, G. I., "A Study of the Causes of the Bauschinger Effect," Doctoral Thesis, M.I.T. (Jan. 1962).

21. Cottrell, A. H., "Dislocations and Plastic Deformation of Crystals," Oxford University Press, p. 112 (1965).

22. Nabarro, F.R.N., "Some Recent Developments in Rheology," British Rheology Club, London (1950).

23. Kulhmann, D., "On Theory of Plastic Deformation," Proc. Phy. Soc. (London), Vol. A64, p. 140 (1951).

24. Seeger, A. and H. Tauble, Z. Metall., Vol. 51, p. 435.

25. Turnbull, J. A., "Comment on Dislocation Climb and Determination of Stacking Fault Energies in Aluminum and Aluminum-1% Magnesium Alloys," J. App. Phys. Vol. 38, p. 4075 (1967).

26. Seeger, A., "Dislocations and Mechanical Properties of Crystals," John Wiley and Sons, New York (1957).

27. Feltner, C. E. and C. Laird, "Cyclic Stress-Strain Response of FCC Metals and Alloys-II, Dislocation Structures and Mechanisms," Acta Met., Vol. 15, p. 1633 (Oct. 1967).

REFERENCES (Concluded)

28. Feltner, C. E. and C. Laird, "Cyclic Stress-Strain Response of FCC Metals and Alloys-I, Phenomenological Experiments," Acta Met., Vol. 15, p. 1621 (Oct. 1967).

29. Thomas, D. A. and B. L. Averbach, "The Early Stages of Plastic Deformation in Cu," Acta Metallurgica, 7, p. 69 (1959).

30. Thomas, G. and J. Washburn, "Electron Microscopy and the Strength of Crystals," Interscience, New York and London (1963).

31. Whelan, M. J., Proc. Roy. Soc., Vol. A249, p. 114.

32. Sankar, N. G., "Unload Emission Behavior of Materials and Its Relation to the Bauschinger Effect," Ph.D. Thesis, The University of Michigan, Ann Arbor, Michigan (1969).

33. Makin, M. J., "Unloading Effects on Plastic Properties of Copper Single Crystals," Phil. Mag. Vol. 3, p. 287 (March 1958).

34. Kelly, E. W. and W. F. Hosford, Jr., "Deformation Characteristics of Textured Magnesium." Trans. Met. Soc. AIME, Vol. 242, p. 654 (April 1968).

35. Segal, R. L. and Partridge, P. G., "Dislocation Arrangements in Aluminum Deformed in Tension or by Fatigue," Phil. Mag., Vol. 4, p. 912 (August 1959).

36. Cottrell, A. H., Trans. Met. Soc. AIME, Vol. 212, p. 192 (1958).